E-8/B-707 Wing Station 320 Transition Fit Fastener Finite Element Analysis

Dr. Gregory A. Shoales, P.E.
Lt Col Scott A. Fawaz, Ph.D., P.E., USAF

Center for Aircraft Structural Life Extension (CAStLE)
Department of Engineering Mechanics

HQ USAFA/DFEM
2354 Fairchild Drive, Suite 2J2
USAF Academy CO 80840-6240
(719) 333-6213, DSN 333-6213

March 2004

DISTIBUTION A: Approved for public release, distribution is unlimited.

DEAN OF THE FACULTY
UNITED STATES AIR FORCE ACADEMY
COLORADO 80840

REPORT DOCUMENTATION PAGE

Form Approved
OMB No. 0704-0188

The public reporting burden for this collection of information is estimated to average 1 hour per response, including the time for reviewing instructions, searching existing data sources, gathering and maintaining the data needed, and completing and reviewing the collection of information. Send comments regarding this burden estimate or any other aspect of this collection of information, including suggestions for reducing the burden, to Department of Defense, Washington Headquarters Services, Directorate for Information Operations and Reports (0704-0188), 1215 Jefferson Davis Highway, Suite 1204, Arlington, VA 22202-4302. Respondents should be aware that notwithstanding any other provision of law, no person shall be subject to any penalty for failing to comply with a collection of information if it does not display a currently valid OMB control number.
PLEASE DO NOT RETURN YOUR FORM TO THE ABOVE ADDRESS.

1. REPORT DATE *(DD-MM-YYYY)*	2. REPORT TYPE	3. DATES COVERED *(From - To)*
17-03-2004	Technical Report	Nov 03-Jan 04

4. TITLE AND SUBTITLE
E-8/B-707 Wing Station 320 Transition Fit Fastener Finite Element Analysis

5a. CONTRACT NUMBER
F05611-03-D-003

5b. GRANT NUMBER

5c. PROGRAM ELEMENT NUMBER

6. AUTHOR(S)
Dr. Gregory A. Shoales, P.E.
Lt Col Scott A. Fawaz, Ph.D., P.E., USAF

5d. PROJECT NUMBER

5e. TASK NUMBER

5f. WORK UNIT NUMBER

7. PERFORMING ORGANIZATION NAME(S) AND ADDRESS(ES)
Center for Aircraft Structural Life Extension (CAStLE)
Department of Engineering Mechanics, HQ USAFA/DFEM
2354 Fairchild Drive, Suite 2J2, USAF Academy CO 80840-6240

8. PERFORMING ORGANIZATION REPORT NUMBER
USAFA TR 04-04

9. SPONSORING/MONITORING AGENCY NAME(S) AND ADDRESS(ES)
ASC/AAA
2145 Monahan Way
Wright Patterson, OH 45433-7017

10. SPONSOR/MONITOR'S ACRONYM(S)

11. SPONSOR/MONITOR'S REPORT NUMBER(S)

12. DISTRIBUTION/AVAILABILITY STATEMENT
DISTIBUTION A: Approved for public release, distribution is unlimited.

13. SUPPLEMENTARY NOTES

14. ABSTRACT
The stress around a Hi-Lok® installed in structure typical of the upper wing station 320 of a Boeing E-8/B-707 aircraft usi finite element method. The requirement came from the Corrosion Kinetics Group (University of Virginia, UVa) of the Aero Systems Center (ASC), Aeronautical Enterprise Program Office (ASC/AA), Aging Aircraft Division (ASC/AAA) Air Vehicle Health Management program. The specific stress result addressed in this work was in response to the installation of the fastener into the subject structure to include initial pre-load and a mild 4 mil (0.004 in) diametric interference (transition) fi PATRAN was used to define the solid model, element mesh, loads and boundary conditions for analysis by MSC/NASTF MSC/PATRAN was used again for post processing of the model solution to create stress fringe contour plots and to asse validity of the finite element model. The stress contour plots are presented for within approximately two diameters of the multiple planes through the skin thickness for hydrostatic as well as the x, y and z components of the stress tensor. While solution presented here was not the highest precision possible for such an analysis, it was judged to be a good first orde

15. SUBJECT TERMS
transition fit, Hi-Lok, aging aircraft, finite element analysis, finite element method, contact modeling, corrosion kinetics stress, NASTRAN, PATRAN, B707

16. SECURITY CLASSIFICATION OF:			17. LIMITATION OF ABSTRACT	18. NUMBER OF PAGES	19a. NAME OF RESPONSIBLE PERSON
a. REPORT	b. ABSTRACT	c. THIS PAGE			Lt Col Scott A. Fawaz
Unclassified	Unclassified	Unclassified		51	19b. TELEPHONE NUMBER *(Include area code)* 719.333.6266

Reset

Standard Form 298 (Rev. 8/98)
Prescribed by ANSI Std. Z39.18

INSTRUCTIONS FOR COMPLETING SF 298

1. REPORT DATE. Full publication date, including day, month, if available. Must cite at least the year and be Year 2000 compliant, e.g. 30-06-1998; xx-06-1998; xx-xx-1998.

2. REPORT TYPE. State the type of report, such as final, technical, interim, memorandum, master's thesis, progress, quarterly, research, special, group study, etc.

3. DATES COVERED. Indicate the time during which the work was performed and the report was written, e.g., Jun 1997 - Jun 1998; 1-10 Jun 1996; May - Nov 1998; Nov 1998.

4. TITLE. Enter title and subtitle with volume number and part number, if applicable. On classified documents, enter the title classification in parentheses.

5a. CONTRACT NUMBER. Enter all contract numbers as they appear in the report, e.g. F33615-86-C-5169.

5b. GRANT NUMBER. Enter all grant numbers as they appear in the report, e.g. AFOSR-82-1234.

5c. PROGRAM ELEMENT NUMBER. Enter all program element numbers as they appear in the report, e.g. 61101A.

5d. PROJECT NUMBER. Enter all project numbers as they appear in the report, e.g. 1F665702D1257; ILIR.

5e. TASK NUMBER. Enter all task numbers as they appear in the report, e.g. 05; RF0330201; T4112.

5f. WORK UNIT NUMBER. Enter all work unit numbers as they appear in the report, e.g. 001; AFAPL30480105.

6. AUTHOR(S). Enter name(s) of person(s) responsible for writing the report, performing the research, or credited with the content of the report. The form of entry is the last name, first name, middle initial, and additional qualifiers separated by commas, e.g. Smith, Richard, J, Jr.

7. PERFORMING ORGANIZATION NAME(S) AND ADDRESS(ES). Self-explanatory.

8. PERFORMING ORGANIZATION REPORT NUMBER. Enter all unique alphanumeric report numbers assigned by the performing organization, e.g. BRL-1234; AFWL-TR-85-4017-Vol-21-PT-2.

9. SPONSORING/MONITORING AGENCY NAME(S) AND ADDRESS(ES). Enter the name and address of the organization(s) financially responsible for and monitoring the work.

10. SPONSOR/MONITOR'S ACRONYM(S). Enter, if available, e.g. BRL, ARDEC, NADC.

11. SPONSOR/MONITOR'S REPORT NUMBER(S). Enter report number as assigned by the sponsoring/ monitoring agency, if available, e.g. BRL-TR-829; -215.

12. DISTRIBUTION/AVAILABILITY STATEMENT. Use agency-mandated availability statements to indicate the public availability or distribution limitations of the report. If additional limitations/ restrictions or special markings are indicated, follow agency authorization procedures, e.g. RD/FRD, PROPIN, ITAR, etc. Include copyright information.

13. SUPPLEMENTARY NOTES. Enter information not included elsewhere such as: prepared in cooperation with; translation of; report supersedes; old edition number, etc.

14. ABSTRACT. A brief (approximately 200 words) factual summary of the most significant information.

15. SUBJECT TERMS. Key words or phrases identifying major concepts in the report.

16. SECURITY CLASSIFICATION. Enter security classification in accordance with security classification regulations, e.g. U, C, S, etc. If this form contains classified information, stamp classification level on the top and bottom of this page.

17. LIMITATION OF ABSTRACT. This block must be completed to assign a distribution limitation to the abstract. Enter UU (Unclassified Unlimited) or SAR (Same as Report). An entry in this block is necessary if the abstract is to be limited.

This page

intentionally

left blank

This technical report, E-8/B-707 Wing Station 320 Transition Fit Fastener Finite Element Analysis, is presented as a competent treatment of the subject, worthy of publication. The United States Air Force Academy vouches for the quality of the research, without necessarily endorsing the opinions and conclusions of the authors. Therefore, the views expressed in this article are those of the authors and do not reflect the official policy or position of the United States Air Force, Department of Defense, or the US Government.

This report has been cleared for open publication and public release by the appropriate Office of Information in accordance with AFI 61-202 and USAFA FOI 190-1. This report may have unlimited distribution.

Prepared by:

17 MAR 04
Date

GREGORY A. SHOALES, Ph.D., PE
Senior Research Engineer,
Center for Aircraft Structural Life Extension

The report has been reviewed and is approved for publication.

18 Mar 04
Date

SCOTT A. FAWAZ, Lt Col, USAF
Director, Center for Aircraft Structural Life Extension

6 May 04
Date

ROBERT S. FREDELL, Lt Col, USAF
Director of Faculty Research

This page

intentionally

left blank

Abstract

The stress around a Hi-Lok® installed in structure typical of the upper wing station 320 of a Boeing E-8/B-707 aircraft using the finite element method. The requirement came from the Corrosion Kinetics Group (University of Virginia, UVa) of the Aeronautical Systems Center (ASC), Aeronautical Enterprise Program Office (ASC/AA), Aging Aircraft Division (ASC/AAA) Air Vehicle Health Management program. The specific stress result addressed in this work was in response to the installation of the Hi-Lok® fastener into the subject structure to include initial pre-load and a mild 4 mil (0.004 in) diametric interference (transition) fit. MSC/PATRAN was used to define the solid model, element mesh, loads and boundary conditions for analysis by MSC/NASTRAN. MSC/PATRAN was used again for post processing of the model solution to create stress fringe contour plots and to assess the validity of the finite element model. The stress contour plots are presented for within approximately two diameters of the fastener at multiple planes through the skin thickness for hydrostatic as well as the x, y and z components of the stress tensor. While the solution presented here was not the highest precision possible for such an analysis, it was judged to be a good first order analysis which met the immediate need of the corrosion kinetics group. Several areas of improvement were suggested for follow on work in this area as requirements dictate a higher fidelity solution.

Contents

Abstract 1
Contents ii
List of Figures iii
List of Tables v
1. Background 1
2. FEM Modeling and Analysis 3
   2.1 Solid model definition 3
   2.2 Finite Element Mesh Generation 6
   2.3 Loads and Boundary Conditions 10
   2.4 Materials and Properties Definition 13
   2.5 Analysis 15
3. Results 16
   3.1 Result Case 1 – Hi-Lok Pre-Load with a Clean fit (no pin interference) 16
   3.2 Result Case 2 – Hi-Lok Pre-load with 0.004 in Diametric Interference Fit 16
4. Discussion 37
5. Conclusion and Recommendations 39
6. References 41

List of Figures

Figure 1: Top view sketch of pin, skin and stiffener solid models with respect to axis system, remote skin stress and edge boundary conditions. Section cuts of solid models shown in Figure 2 and 3 are indicated. 4
Figure 2: Section A-A from Figure 1 of pin (blue), skin (green) and stiffener (yellow) solid models showing MSC/PATRAN global coordinate system. 5
Figure 3: Section B-B from Figure 1 of pin (blue), skin (green) and stiffener (yellow) solid models showing MSC/PATRAN global coordinate system. 5
Figure 4: Samples of congruent solids used to construct the present work's three solid elements (pin, skin and stiffener) showing a) pin b) bottom side of stiffener on skin c) top side of skin on stiffener and d) close up of skin countersunk hole. 6
Figure 5: Examples of MSC/PATRAN mesh seeds and the resulting mesh for the a) pin and the b) stiffener and skin model components. 8
Figure 6: Drop down menu used to easily create lists in MSC/PATRAN. 9
Figure 7: Shareware utility provided with MSC/PATRAN to quickly create gap elements. 9
Figure 8: Example of a single set of slide line contact curves on their associated solid model components. 11
Figure 9: Thickness plane location of MSC/PATRAN *Results* stress fringe contour plots. 16
Figure 10: Hi-Lok pre-load with a clean fit, hydrostatic stress contour plot of top plane thickness location. 17
Figure 11: Hi-Lok pre-load with a clean fit, stress tensor x-component contour plot of top plane thickness location. 17
Figure 12: Hi-Lok pre-load with a clean fit, stress tensor y-component contour plot of top plane thickness location. 18
Figure 13: Hi-Lok pre-load with a clean fit, stress tensor z-component contour plot of top plane thickness location. 18
Figure 14: Hi-Lok pre-load with a clean fit, hydrostatic stress contour plot of ¼ t plane thickness location. 19
Figure 15: Hi-Lok pre-load with a clean fit, stress tensor x-component contour plot of ¼ t plane thickness location. 19
Figure 16: Hi-Lok pre-load with a clean fit, stress tensor y-component contour plot of ¼ t plane thickness location. 20
Figure 17: Hi-Lok pre-load with a clean fit, stress tensor z-component contour plot of ¼ t plane thickness location. 20
Figure 18: Hi-Lok pre-load with a clean fit, hydrostatic stress contour plot of ½ t plane thickness location. 21
Figure 19: Hi-Lok pre-load with a clean fit, stress tensor x-component contour plot of ½ t plane thickness location. 21
Figure 20: Hi-Lok pre-load with a clean fit, stress tensor y-component contour plot of ½ t plane thickness location. 22
Figure 21: Hi-Lok pre-load with a clean fit, stress tensor z-component contour plot of ½ t plane thickness location. 22
Figure 22: Hi-Lok pre-load with a clean fit, hydrostatic stress contour plot of ¾ t plane thickness location. 23
Figure 23: Hi-Lok pre-load with a clean fit, stress tensor x-component contour plot of ¾ t plane thickness location. 23

Figure 24: Hi-Lok pre-load with a clean fit, stress tensor y-component contour plot of ¾ t plane thickness location. 24
Figure 25: Hi-Lok pre-load with a clean fit, stress tensor z-component contour plot of ¾ t plane thickness location. 24
Figure 26: Hi-Lok pre-load with a clean fit, hydrostatic stress contour plot of bottom plane thickness location. 25
Figure 27: Hi-Lok pre-load with a clean fit, stress tensor x-component contour plot of bottom plane thickness location. 25
Figure 28: Hi-Lok pre-load with a clean fit, stress tensor y-component contour plot of bottom plane thickness location. 26
Figure 29: Hi-Lok pre-load with a clean fit, stress tensor z-component contour plot of bottom plane thickness location. 26
Figure 30: Hi-Lok pre-load with a 0.004 in interference fit, hydrostatic stress contour plot of top plane thickness location. 27
Figure 31: Hi-Lok pre-load with a 0.004 in interference fit, stress tensor x-component contour plot of top plane thickness location. 27
Figure 32: Hi-Lok pre-load with a 0.004 in interference fit, stress tensor y-component contour plot of top plane thickness location. 28
Figure 33: Hi-Lok pre-load with a 0.004 in interference fit, stress tensor z-component contour plot of top plane thickness location. 28
Figure 34: Hi-Lok pre-load with a 0.004 in interference fit, hydrostatic stress contour plot of ¼ t plane thickness location. 29
Figure 35: Hi-Lok pre-load with a 0.004 in interference fit, stress tensor x-component contour plot of ¼ t plane thickness location. 29
Figure 36: Hi-Lok pre-load with a 0.004 in interference fit, stress tensor y-component contour plot of ¼ t plane thickness location. 30
Figure 37: Hi-Lok pre-load with a 0.004 in interference fit, stress tensor z-component contour plot of ¼ t plane thickness location. 30
Figure 38: Hi-Lok pre-load with a 0.004 in interference fit, hydrostatic stress contour plot of ½ t plane thickness location. 31
Figure 39: Hi-Lok pre-load with a 0.004 in interference fit, stress tensor x-component contour plot of ½ t plane thickness location. 31
Figure 40: Hi-Lok pre-load with a 0.004 in interference fit, stress tensor y-component contour plot of ½ t plane thickness location. 32
Figure 41: Hi-Lok pre-load with a 0.004 in interference fit, stress tensor z-component contour plot of ½ t plane thickness location. 32
Figure 42: Hi-Lok pre-load with a 0.004 in interference fit, hydrostatic stress contour plot of ¾ t plane thickness location. 33
Figure 43: Hi-Lok pre-load with a 0.004 in interference fit, stress tensor x-component contour plot of ¾ t plane thickness location. 33
Figure 44: Hi-Lok pre-load with a 0.004 in interference fit, stress tensor y-component contour plot of ¾ t plane thickness location. 34
Figure 45: Hi-Lok pre-load with a 0.004 in interference fit, stress tensor z-component contour plot of ¾ t plane thickness location. 34
Figure 46: Hi-Lok pre-load with a 0.004 in interference fit, hydrostatic stress contour plot of bottom plane thickness location. 35

Figure 47: Hi-Lok pre-load with a 0.004 in interference fit, stress tensor x-component contour plot of bottom plane thickness location. 35
Figure 48: Hi-Lok pre-load with a 0.004 in interference fit, stress tensor y-component contour plot of bottom plane thickness location. 36
Figure 49: Hi-Lok pre-load with a 0.004 in interference fit, stress tensor z-component contour plot of bottom plane thickness location. 36
Figure 50: Stress contour plot for Hi-Lok pre-load and interference fit load case with MSC/PATRAN *Results* averaging disabled for the von Mises stress solution. 38
Figure 51: Element to element node solution maximum difference for Hi-Lok pre-load with interference fit load case. Stress tensor, y-component contour plots of a) top view isometric and b) x-z plane at y=0. 38

List of Tables

Table 1: MSC/PATRAN mesh seed summary. 7
Table 2: Summary of isotropic linear elastic material properties used in FEM model. 13
Table 3: Summary of key MSC/PATRAN *Analysis* parameter assignments required for FEM model convergence. 15
Table 4: Summary of comparisons between element to element node solutions and the stress result for the same location. Hi-Lok pre-load with interference fit load case. 39

This page

intentionally

left blank

1. Background

The Air Vehicle Health Management (AVHM) Program's corrosion kinetics group at University of Virginia's Center for Electrochemical Science and Engineering (CESE) needs to know stress field details in the immediate vicinity of a transition fit fastener. Their work, while aimed at a host of aging aircraft corrosion problems, is currently focused on the upper wing skin of the Boeing E-8C JOINTSTARS aircraft. This is the same airframe which is known commercially as the Boeing B-707. The Center for Aircraft Structural Life Extension (CAStLE) at the United States Air Force Academy (USAFA) used their in house finite element analysis (FEA) expertise to answer this need. The CAStLE in house MSC/PATRAN solid modeling capability can easily create detailed multi component solid models. This program easily prepares the solid models for analysis by MSC/NASTRAN using the finite element method (FEM).

CESE's directors [1] wish to establish tensile stress location and orientation near the fastener. Depending on their location and relative magnitude, they have the potential to accelerate the intergranular (IG) corrosion into stress-corrosion cracking. While the goal of any stress analysis is to achieve the highest precision possible, the CESE group is most concerned with understanding the relative magnitudes and direction of tensile stresses. One of their goals for our FEA results is to be able to compare the stresses generated by the installation of the transition fit fastener with the stresses generated by corrosion product accumulation between the grains as IG corrosion occurs. The spatial distribution of both stresses, when compared to the shape of the IG attack region around the fastener will help determine to what extent the installation stresses might affect the IG corrosion.

The specific fastener was defined by the AVHM Program's focus structure--upper wing station (WS) 320. This location therefore defines the geometry, materials and loads of the problem to be modeled. The fastened members are a 0.18 in thick Al 7178-T6 wing skin fastened to a 0.07 in thick Al 7075-T6 stiffener cap. Based on samples provided by the aircraft depot the fastener type is an HL19-10 (5/16 in nominal diameter) 100° countersunk Hi-Lok with a 0.25 in nominal grip range. Per the Boeing Structural Repair Manual (SRM) [2], the fastener hole diameter specification is 0.309 to 0.313 in. The HL19-10 pin diameter specification [3] is between 0.311 and 0.312 in. Taken together, the hole and pin specification translate to the fastener being installed as either a loose fit with no net interference or a transition fit with up to a 3 mil interference. In order to err to the conservative in this initial work, the interference was taken to be 4 mil (0.004 in). The remote stress applied to the skin in that WS vary from positive 16.8 KSI to negative 28 KSI. The load transferred into the stiffener is 6 to 7%.

While the remote stress and the load transfer are necessary to fully model the problem, the corrosion kinetics team's [4] current interest is the fastener near field stress (within 2 diameters) developed by the installation of the HL19-10 Hi-Lok in the subject structure. The following work therefore focuses on the state of stress near the fastener in response to the installation torque with and without the maximum possible interference fit. Also per the corrosion kinetics team, the stress field is reported as hydrostatic stress, and normal stress for both the skin plane direction and the skin normal direction. These stress results are reported at the top surface, mid-plane, bottom surface and two additional planes in between.

MSC/PATRAN post processing tools were used to judge the convergence and therefore the validity the solutions obtained.

2. FEM Modeling and Analysis

The following sections detail the development of the FEM model using MSC/PATRAN. The order of presentation follows the order that might be taken by a user of this software. All analysis was performed using MSC/NASTRAN. While MSC/PATRAN makes the creation of complex geometry fairly simple, there exist certain limitations in the analysis capabilities of MSC/NASTRAN's when applied to problems such as this. Prime examples of these limitations are in the area of large multi-axis solid model contact and the non-linear MSC/NASTRAN solver necessary to address them. Some of the modeling steps in the following sections are therefore presented purely to minimize such analysis limitations thereby obtaining the most reasonable solution using the tools available within CAStLE at the time of this work

2.1 Solid model definition

The first step in the FEA process is to determine what solids need to be modeled and what interactions exist between them. The "plate with a hole in it" problem has been modeled by even the most junior FEM student. In the case of an installed fastener in that hole, the interaction between the fastener and the hole edge has the potential to dramatically change the solution. The pin to skin interaction will obviously be important in the case of an interference fit during initial pin installation. It will also impact the result when remote stresses cause local deformation around the hole. The pin will restrain the deformation of the skin in the direction of the pin. The level of restraint will be governed by the relative difference in the stiffness of the pin compared to the skin. Since the steel HL19 Hi-Lok has three times the stiffness of the surrounding aluminum structure, this restraint is not trivial. An unsymmetric joint may also introduce rivet rotation and relative sliding between the attached members.

The next consideration is the installation of the Hi-Lok collar. By design these collars install on the pin with a preset torque. The recommendation for the HL19 pin is the HL70 collar. According to the manufacturer [3] the HL70-10 collar installs with between 130 and 160 in-lb of torque. The installation torque creates the Hi-Lok installation preload or clamping force. With a countersunk fastener the clamping force manifests by equal and opposite forces (towards each other) applied by the pin countersink head's contact with the skin countersink surface and the contact patch between the collar and the stiffener cap. The installation at hand, as with most, also includes a washer between the collar and the stiffener cap. The washer surface therefore defines the contact patch on the stiffener cap. Stress resulting from the clamping force is transmitted into the skin not only through the force applied in the contact between the pin and skin countersink contact but also through contact between the skin and the stiffener. The degree of contact will vary depending on the aforementioned local deformation in response to the applied loads of the hole around the pin.

The remote stress on the skin is also an important part of the complete state of stress near a fastener. The skin may deform in response to the remote stress. As already observed the presence of the stiffer pin in the hole offers restraint to deformation near the hole. Additionally, the fastener itself transfers a portion of that stress to the stiffener. This load

transfer is a function of the relative stiffness of both components, the relative sizes of both components and also the manner of contact between those components.

The FEA model will consist on three separate solid model components; the pin, the stiffener, and the skin. The pin dimensions in diameter and countersink dimensions match those of Hi-Lok. Because of the way the loads will be applied (described later), the pin shank will be limited to the grip length or 0.25 in from the top of the head. The MSC/PATRAN global model axis origin will be at the top of the pin's head on the center axis. The positive z-axis will extend up away from the pin. The positive x-axis will be aligned with the direction of the remote stress while the y-axis will be transverse to that stress. The skin was a plate with a countersink matching that of the pin. The top surface of the plate is located at the z=0 while the bottom surface of the plate is located at z=0.18 in. The plate was made sufficiently long in the axial (x-axis) direction so as to preclude edge effects from the remote stress application or boundary conditions. A distance of approximately 50 diameters in the ±x direction was chosen. The width (y-axis direction) was also sufficiently long to avoid edge effects but was more importantly tailored to achieve the desired load transfer. As will be described later, a load transferred of 6.5% into the stiffener was obtained if the skin was 7.5 in wide. Taken all together the skin solid model is a plate from z=0 to z=−0.18 in, x=±15.75 in, and y=±3.75 in. The stiffener solid model was an additional solid plate with a hole on the z-axis matching the pin shank diameter of 0.312 in. The length in the axial direction was the same as the skin solid model. The width was chosen to accomplish two things. First, it needed to be sufficiently wide to transfer the Hi-Lok preload from the collar/washer contact patch through to the skin. Second, the stiffener width compared to the skin width is one of the factors which determine the amount of load transferred into the stiffener from the skin. The thickness was of course chosen to match the subject structure and fastener grip range. Taken all together the stiffener solid model is a plate from z=−0.18 to −0.25 in, x=±15.75 and y=±0.75. the sketch in Figure 1 summarizes the solid models used for this FEA and indicated the x and y-axis relative to remote stress and edge boundary condition (discussed later).

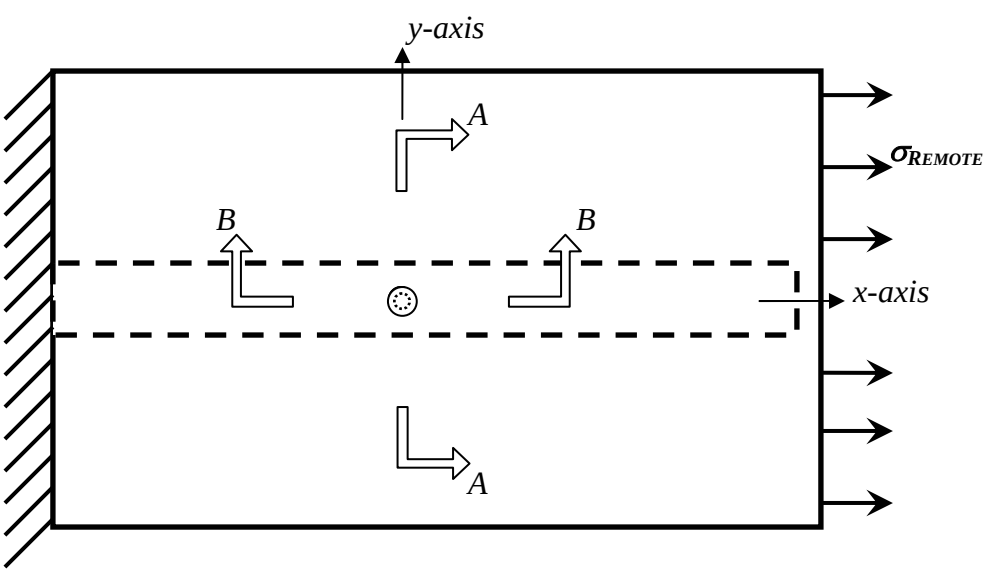

Figure 1: Top view sketch of pin, skin and stiffener solid models with respect to axis system, remote skin stress and edge boundary conditions. Section cuts of solid models shown in Figure 2 and 3 are indicated.

Detailed section views of the fastener near field are shown in Figures 2 and 3. Theses sections are specified in Figure 1. The MSC/PATRAN global coordinate system indicated in these figures is used throughout the current work.

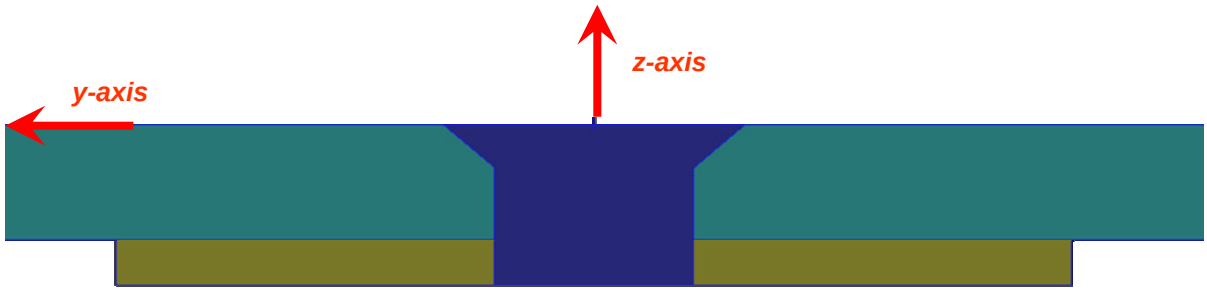

Figure 2: Section A-A from Figure 1 of pin (blue), skin (green) and stiffener (yellow) solid models showing MSC/PATRAN global coordinate system.

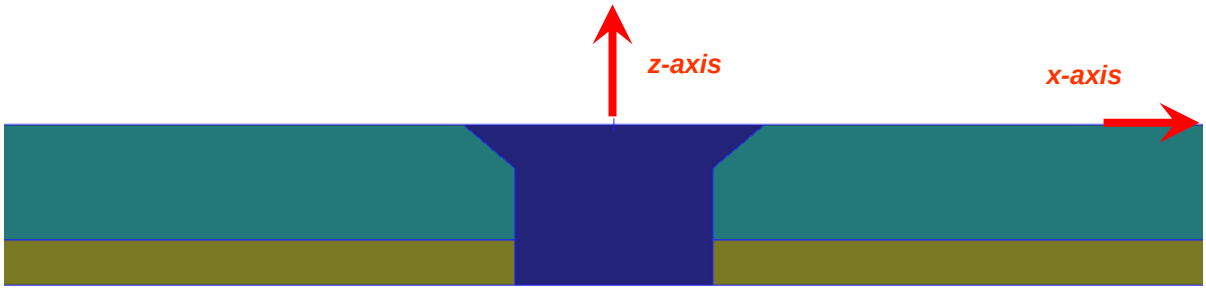

Figure 3: Section B-B from Figure 1 of pin (blue), skin (green) and stiffener (yellow) solid models showing MSC/PATRAN global coordinate system.

Reviewing the solid model configuration just presented and the loading that will ultimately be included in this model, several areas of direct contact will clearly exist. MSC/NASTRAN models contact in one of two ways; slide lines and gap elements. Contact details will be fully discussed in Section 2.3 but the relevant item here is that both methods require the contacting solids to have either coincident nodes or sets of matching sets of nodes with some finite (small) separation. In this work the contacting solids will have sets of coincident nodes. In order to make this possible the mesh had to be generated uniformly across the gaps between the contacting solids. The easiest way to do this is using the MSC/PATRAN automatic *IsoMesher*. Accordingly, all of the models components were created under the requirements of the parametrically defined solid [5]. The easiest way to accomplish this was to extrude surfaces composed of no more than 4 sides through a specified thickness. Each of the model components were composed of several of these congruent solids. Since the *IsoMesher* defines FEM elements between solid boundaries, separate solids were also defined used to create element boundaries in order to facilitate other FEA model development steps. One example of this was the surface where the Hi-Lok collar pre-load would be applied to the stiffener. Defining the stiffener solids such that their shape on the bottom surface (z=−0.25 in) matches the where the collar/washer applies its pre-load makes applying that pre-load far easier to accomplish. Figure 4 shows some of the details of the congruent solids used for the three model components (pin, skin and stiffener) used in this work. Each component can be distinguished by the same colors given in Figures 2 and 3. Additionally, to simplify further

model development, each of the three component were put in separate MSC/PATRAN groups—namely the pin, skin and stiffener groups.

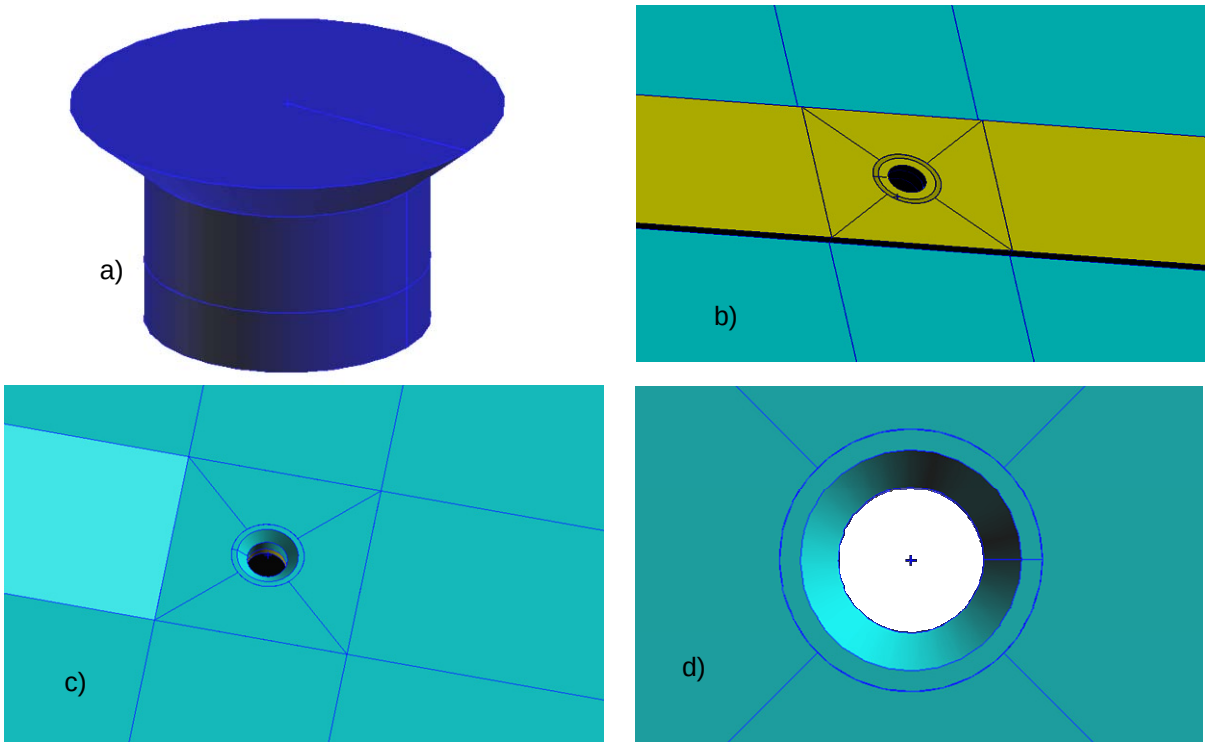

Figure 4: Samples of congruent solids used to construct the present work's three solid elements (pin, skin and stiffener) showing a) pin b) bottom side of stiffener on skin c) top side of skin on stiffener and d) close up of skin countersunk hole.

2.2 Finite Element Mesh Generation

2.2.1 Solid Elements

Before beginning the MSC/PATRAN mesh generation process, the type of element must be selected. Again, the requirement for modeling contact dictates the need for coincident nodes on surfaces of contacting model elements. Quadrilateral solid MSC/NASTRAN Hex solid elements were selected for this very reason. Hex elements are very easily defined in uniform layers. It is consequently very easy to match layers from one solid to another given the right control during mesh generation. Some element boundaries are already defined by the congruent solids as described in Section 2.1. Since the solids of each component were designed with matching boundaries where they contact each other so to will the element mesh boundaries match on contacting surfaces. These matching solid surfaces are evident when comparing the views in Figure 4. In between those solid boundaries the mesh can be controlled using the MSC/PATRAN ***Elements****:Create:Mesh*[1] *Seed* tool. These "seeds" specify where element corner nodes must be located thereby forcing the mesh generator to a preset mesh density. A mesh seed is selected around the hole circumference, across the countersink, down the hole bore and around other edges of the contact surfaces (as shown in

[1] Convention used throughout this work to refer to the use MSC/PATRAN tools. The bold first word (***Elements***) refers to one of the eleven Main Menu buttons from ***Geometry*** to ***XY Plot***.

Figure 5). The identical seed was established on both sides of the contacting surfaces. The final consideration in element selection was the realization that contact analysis requires a nonlinear solution of the FEM model. The only MSC/NSATRAN Hex elements are the Hex 8 solid elements. These six-sided elements have nodes at each of the eight corners—hence the Hex 8 name.

The MSC/PATRAN mesh seeds are applied to curves which define the boundaries of solids. The specific mesh seeds applied to the components of the FEM model are summarized in Table 1.

Table 1: MSC/PATRAN mesh seed summary.

model components	element density	location
pin, skin	48	hole circumference at top of countersink (z=0), bottom of countersink (z=−0.063), bottom of skin (z=−0.18)
pin, stiffener	48	hole circumference at top of stiffener (z=−0.18), bottom of stiffener (z=−0.25)
pin, skin	4	radial direction along countersink (y=0, x=0.156 to 0.236, z=0 to −0.063)
skin, stiffener	6	under collar/washer contact patch (x=0.156 to 0.28, y=0, z=−0.25)
pin, skin	8	down shank portion of hole bore (x=0.156, y=0, z=−0.063 to −0.18)
pin, stiffener	4	down the hole bore (x=0.156, y=0, z=−0.18 to −0.25)
skin, stiffener	6	The 4 diagonals extending from circular solids around hole to the edge of central square around the hole

With these seeds in place each solid was meshed using the MSC/PATRAN default settings for remaining element density decisions. After mesh generation was complete each MSC/PATRAN group was “equivalence”. The MSC/PATRAN ***Elements****:Equivalence:Group* tool equivalences all nodes in the selected group by eliminated duplicate nodes created when congruent solids are meshed. In other words, when two adjoining elements are made in two separate—even congruent—solids, the mesh generator creates separate nodes for each one. The equivalence tool eliminates the duplicate nodes to create a continuous solid mesh. By using the MSC/PATRAN equivalence tool on the nodes by group a solid model was created with three distinctly separate solid components. Figure 5 shows the mesh seeds from Table 1 along with the resulting solid element mesh. The seed locations are shown by the yellow circles.

2.2.2 Bar Elements

The next element type generated is associated with the contact modeling. MSC/NASTRAN gap elements are well suited for plane surface to plane surface contact where the displacement will be normal (or nearly so) to those surfaces. In the current work such contact exists between the skin and the stiffener (z=−0.18) when the two components are

clamped together by the Hi-Lok pre-load. The first step in defining gap elements was to create a one-dimensional (1-D) bar element between the coincident nodes on the area of contact. These bar elements could have simply been established between all coincident nodes over the entire contact surface. However, previous worked [6] showed that the effect of the Hi-Lok's preload is limited to the fastener near-field rather than the entire 31.5 in of stiffener length. Limiting the contact model to this fastener near field eliminates needless degrees of freedom (***DoF***) in the model. For this work therefore the gap elements were only defined between the skin and stiffener in the square area around the hole between x, y=±1.5 in (see Figure 4b). The validity of the abbreviated contact area was also verified after the FEM solution was obtained. If the coincident nodes of the contact surfaces displace relative to each other such that penetration was indicated, the gap element surface was too small. As will be discussed later, this was not the case and the contact surface chosen for the gap elements was appropriate.

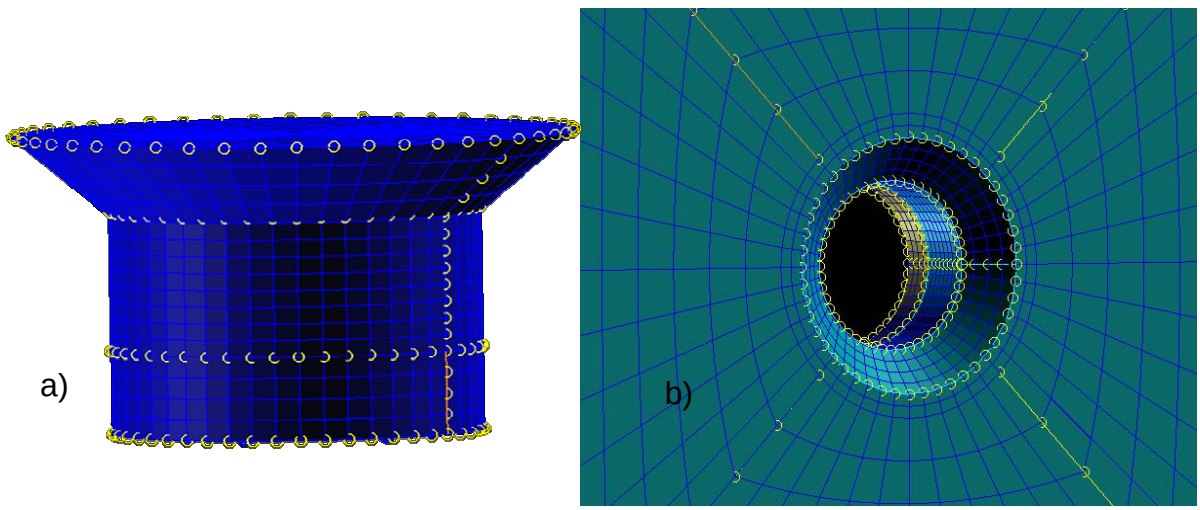

Figure 5: Examples of MSC/PATRAN mesh seeds and the resulting mesh for the a) pin and the b) stiffener and skin model components.

Even though the gap element contact area was greatly reduced it still represented 624 coincident nodes pairs. Creating 624 bar elements manually would be a formidable task to say the least! Fortunately two MSC/PATRAN tools made this task quick and painless. While this work is by no means intended to take the place of MSC/PATRAN training, the utility of these tools make them worth highlighting. The first was to use the *Tools:List:Create*[2] drop-down menu to create two lists of nodes. The first of all skin group nodes at z=−0.18 in and between x, y=±1.5 in and the other of all stiffener group nodes in the same coordinate range. Access to this tool through the MSC/PATRAN drop down menus is shown in Figure 6. Once the user selects this tool as shown in Figure 6, it is simply a matter of posting the appropriate group (skin or stiffener) and using the MSC/PATRAN graphical picking tools to select the desired set of nodes.

The other tool is part of the shareware tools provided with MSC/PATRAN and accessed under the *Utilities:FEM-elements:Create 1-D Gap Elements* drop-down menu. The nodes

[2] Further convention used throughout this work to refer to the use MSC/PATRAN tools. The non-bold first word (*Tools*) refers to one of the ten drop-down menus from *File* to *Utilities*.

sets just created with the *Tools:List:Create* tool are added to the appropriate dialog boxes as shown in Figure 7. Using the specified tolerance this utility automatically creates bar elements connecting the two closest nodes between each set. Another helpful step in the element mesh creation step is done after the mesh is created and the individual component groups have their nodes equivalenced. Another technique that is extremely helpful is to renumber the nodes and elements in each group by some convenient number system which will later be indicative of that group. For example, depending on the number of elements in each group, one could have its nodes and elements numbered from 1 to 1000, the next could have all nodes and elements numbered from 10,000 to 20,000, and so on. Again, MSC/PATRAN provides an easy to use tool under the *Elements* tools. Each group is posted one at a time and the ***Elements****:Renumber:Node* and ***Element****:Renumber:Element* options are selected giving some starting number for each set. Having done this it becomes a simple matter to ensure that nodes or elements in a large model come from the desired model component—such as during the aforementioned list creation step. This renumbering step also came in handy latter on when evaluating the model's solution.

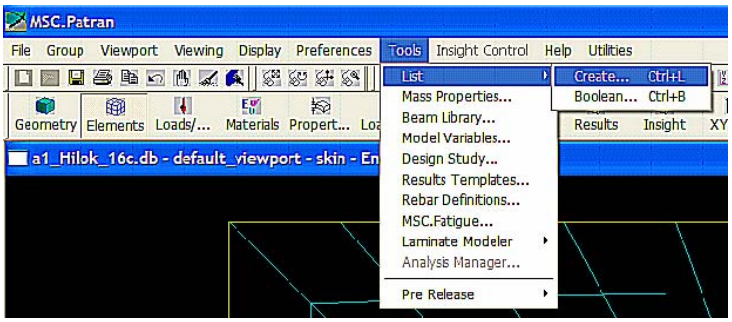

Figure 6: Drop down menu used to easily create lists in MSC/PATRAN.

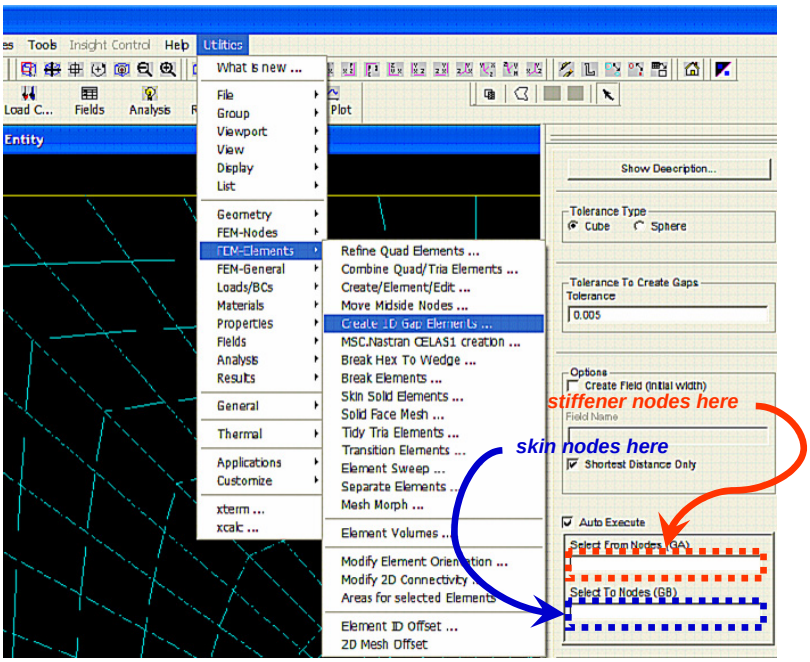

Figure 7: Shareware utility provided with MSC/PATRAN to quickly create gap elements.

2.3 Loads and Boundary Conditions

The following section describes in detail the loads that were necessary to model the structure of interest. Each load type was combined with the applicable restraint (boundary conditions) under MSC/PATRAN ***Load Cases***. The ***Load Cases*** are then selected for analysis in various combinations to represent the different possible load environments for the HL19 Hi-Lok at WS 320. Load case selection in the MSC/PATRAN ***Analysis*** tool also re-created the actual sequence of load application with their matching boundary conditions, During the model analysis each of these ***Load Cases*** were analyzed as a separate *subcase* by MSC/NASTRAN.

2.3.1 Slide Line Contact

The first boundary condition to be discussed is associated with the other region of contact in the global model. That is the surface of the hole between the pin and the skin/stiffener combination. This boundary condition was present in <u>all</u> load cases. Gap elements were initially tried for this contact region but latter discarded. The reason was that little success was found using MSC/NASTRAN gap elements for any surfaces that might have a degree of sliding. In other words if a surface of gap element nodes did anything but uniformly directly approach or directly move away from the opposing surface of nodes the solution was suspect. In the extreme such transverse motion would prevent the analysis from converging to any solution at all. This observation was despite the fact that available property assignments for the gap elements seemed to take transverse motion into account [7]. While these transverse properties could be assigned, doing so did not help convergence nor did it seem to accurately model the situation. Adams and Askenazi [8] confirm this observation and refer to gap elements as "…point-to-point connections that behave as conditional spring dampers." They go on to describe the other way to model contact as what MSC/NASTRAN calls slide line contact. These lines of contact not only permitted transverse motion along the contact but are also particularly suited to non-uniform motion between opposing surfaces. This was exactly what the MSC application engineers ultimately recommended for this type of contact.

Unlike the easy tools for creating vast fields of gap elements, creating slide lines under MAC/Patran was an extremely time consuming process. Slide line contact is a 2-dimensional (2-D) boundary condition. In the 2-D model they would be established as opposing lines on the edges of 2-D model that would be in contact. In order to make them work between surfaces of a 3-D model a number of these opposing slides lines need to be combined together in a field between each of the model surfaces. The associated MSC/NASTRAN card that defines the contact lines by a series of nodes which lay along the opposing contact lines on each surface. Accordingly, some pre-planning must take place during mesh generation to ensure nodes exist on both surfaces along the (same) desired line of contact. MSC/NASTRAN refers to one curve as the "Slave" while the opposing curve on the other surface is called the "Master". Consistency is required between the surfaces having a set of Slave curves and the surfaces having the set of Master curves. Another wrinkle in the process is that MSC/Patran only permits the specification of contact by geometric curves (rather than a series of nodes). Separate curves must therefore be generated on each surface and the desired nodes must be connected (called associated by MAC/Patran) with those curves. For reasons that remain unclear, the opposing curves cannot be the same length so this also must be taken into account when creating the curves.

As an example the following illustrates the creation of one such contact slide line used on this project. Consider for this example the contact on the x-axis between the pin and skin/stiffener. In a top down view and using the central axis of the pin as a reference, this was referred to as the 0° line of contact. Previous mesh seeding ensures a line of nodes exist at this location on both surfaces. A slave curve was defined on the pin surface. Since both surfaces are equal length, the slave curve was extended from the top out to an arbitrary point in space—satisfying MSC/PATRAN's requirement that the curves not be exactly equal in length. A master curve was also defined spanning both the skin and the stiffener surfaces. Both curves are continuous—in other words the countersunk portion is joined with the straight shank portion to create a single curve. The ***Elements***:*Associate:Nodes:Curve* tool is then used to connect the slave curve to the 17 nodes on the pin's surface. The tool is used again to associate the master curve to the 17 nodes on the opposing skin and stiffener surface. Figure 8 shows this set of slide line curves on the model components. The process can be repeated for as many lines of contact as practical—limited by the number of lines of opposing nodes on the solid models. Therefore for this work, there could have been as many as 48 slide lines.

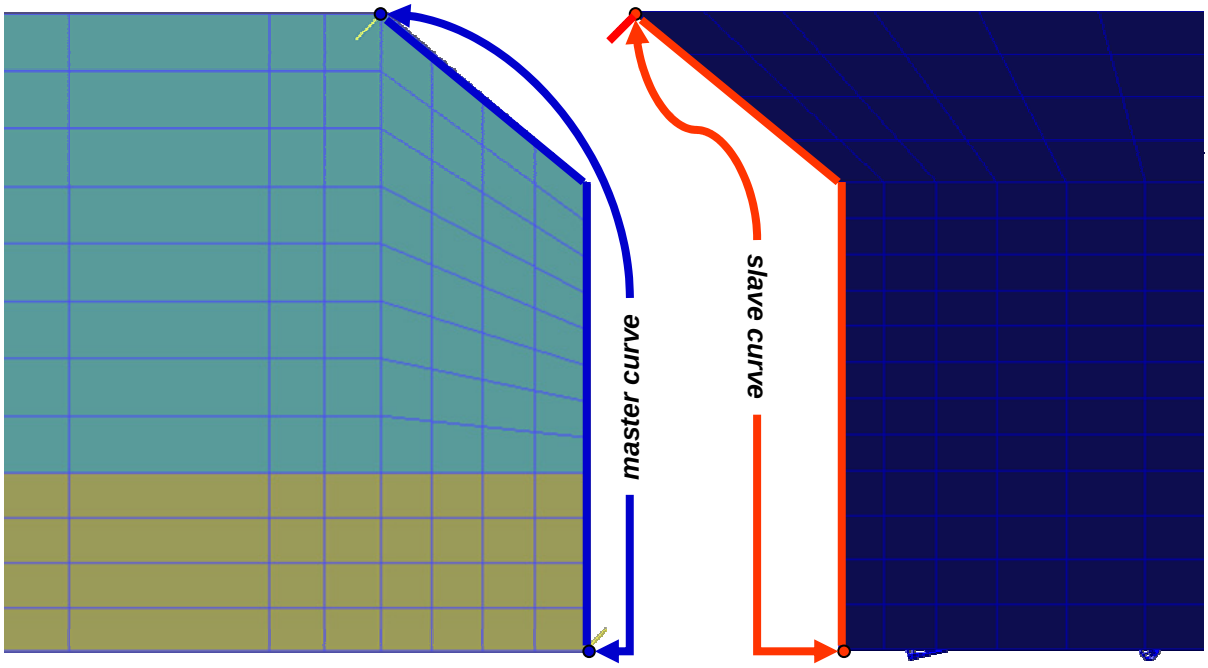

Figure 8: Example of a single set of slide line contact curves on their associated solid model components.

Have successfully associated the slave and master curves with their nodes, the next step is to use the ***Elements***:*Create:Contact* tool. A vector pointing from the master to the slave curve was entered for each set of slide line contacts in the Input Properties dialog box. This vector must have been previously created using the MSC/PATRAN ***Geometry*** tool. Under the Select Application Region dialog box the slave and master curves are selected.

As stated previously this process is repeated for the desired number of contacts. In the present work 16 lines of contact were established at 0, 15, 45, 75, 90, 105, 135, 165, 180, 195, 225, 255, 270, 285, 315 and 345° about the pin central axis. When in active contact,

each slide line essentially behaves as a concentrated load. The number of contacts chose was a compromise between the extraordinarily long time it would take to manually enter all 48 possible and a sufficient number to adequately distribute the contact loads on the surface. Even so, the stress result in the immediate vicinity of the slide lines from the FEM model analysis should be considered just as suspect as a stress result near any other concentration of applied load. The slide line stress concentration effect will be discussed in later sections.

2.3.2 Transition Fit Pin (Load Case 0)

The possible interference between the pin and the drilled hole was modeled by applying a thermal strain to the pin shank. This technique had been use successfully in the past [9] for just this situation. Under the boundary condition assignment the pin is given an initial temperature and a final temperature. Thermal strain ($\boldsymbol{\varepsilon_T}$) is governed by the change in temperature ($\boldsymbol{\Delta T}$) and a material thermal expansion coefficient ($\boldsymbol{\alpha_T}$) through the relationship shown in Equation 1.

$$\varepsilon_T = \alpha_T \cdot \Delta T \tag{1}$$

The amount of strain needed to be modeled is the maximum possible diametric interference of 0.004 in divided by the nominal pin diameter (0.31 in) or 0.013 in/in. A nominal $\boldsymbol{\Delta T}$ of 100°F was selected. Using Equation 1 this meant that $\boldsymbol{\alpha_T}$=130E-6 /°F would yield the desired strain. In order to define this load step the pin shank was assigned an initial temperature of 10°F and a final temperature of 110°F. The thermal expansion coefficient was added during the property assignment step to be discussed later. It is worth noting here that the $\boldsymbol{\alpha_T}$ chosen has no relation the actual for Al 7178 but rather was used as a modeling technique to achieve the desired diametric strain.

In addition to the temperature assignment to the pin shank several displacement constraints were necessary. Most of these served to hold the slide lines in alignment with each other during the incremental application of the thermal strain thereby aiding solution convergence. First, the top of the pin (z=0) was restrained in the z direction at four evenly spaced interior nodes. The pin was also restrained from rotating about the z-axis by pinning two nodes on the x-axis in the y direction. Next, the bottom of the skin (z=−0.18 in) was also restrained in the z direction on the square perimeter around the hole (x, y=±1.5 in). Finally, all skin and stiffener nodes at x=−1.5 in and y=±1.5 in were restrained in all three directions. These restraint conditions mimicked the operation of installing interference fit fasteners and greatly improved the stability of the incremental solutions and therefore sped the model's convergence. In case there is any doubt in their validity it is worth noting that they were removed in subsequent load steps.

2.3.3 Hi-Lok Pre-Load (Load Case 1)

The Hi-Lok pre-load was also present for all load case combinations since it models the installation of the Hi-Lok collar on the pin. This load was simply the initial tension provided by the preset torque which is designed into the Hi-Lok fastener system. It is largely a factor of pin diameter and the installation torque. The Many formula [10, 11] shown in Equation 2 gives this initial bolt pre-load ($\boldsymbol{F_i}$) as function of installation torque ($\boldsymbol{T}$), nominal bold diameter ($\boldsymbol{d_{BOLT}}$) and torque coefficient ($\boldsymbol{K}_\mathrm{T}$) for which a value of 0.2 is commonly used.

$$F_i = \frac{T}{K_T \cdot d_{BOLT}} \tag{2}$$

Referring once again to the Hi-Lok manufacturer's specification [3], values of 0.312 in and 130 in-lb were used for $\boldsymbol{d_{BOLT}}$ and $\boldsymbol{T}$, respectively. Therefore the pre-load value is 2,080 lb. This load is applied to the bottom of the pin in the –z direction—effectively pulling the pin through the skin. It was also applied in the +z direction to element that were created under the washer contact patch on the bottom (z=−0.25 in) of the stiffener.

The boundary conditions associated with this load step where to stabilize the immediate area around the fastener. Specifically, the stiffener top (z=−0.18) was pinned in the z direction again on the square perimeter around the hole (x, y=±1.5 in). Also both the pin and stiffener were fixed in x, y and z at x=−1.5 in and y=±1.5. Additionally, to continue to help the contact slides lines remain aligned with one another the pin was again restrained from rotation about the z-axis. This was accomplished by the same nodal restraint presented in Section 2.3.2.

2.3.4 Remote Stress (Load Case 2)

The final load case modeled was the application of the remote stress as shown in Figure 1. The magnitude of the remote stress was either 16,800 lb/in^2 in tension or 28,000 lb/in^2 in compression—the extremes for WS 320. This stress was applied to the face of the skin elements on the y-z plane at x=15.75 in. The only boundary condition applied to the skin and stiffener for this load case was to restrain the element faces in the x, y and z directions on y-z plane at x=−15.75 in—thereby modeling the fixed edge condition. Also, since the stiffener was restrained on this face, some of the remote skin stress would be transferred into it as previously discussed. The pin rotation restraint was also retained for this load case.

2.4 Materials and Properties Definition

2.4.1 Isotropic Materials

The FEM model consisted of three different sets of material properties. For isotropic linear elastic material properties MSC/NASTRAN requires two of the following three properties be assigned; Young's modulus ($\boldsymbol{E}$), Poisson's ratio ($\boldsymbol{\nu}$) and Shear modulus ($\boldsymbol{G}$). These are assigned using the MSC/PATRAN ***Materials*** tool and then applied to the appropriate elements using the MSC/PATRAN ***Properties*** tool. For this work, $\boldsymbol{E}$ and $\boldsymbol{\nu}$ were selected. Table 2 summarizes the material properties entered and the FEM model component to which they were applied. Aluminum properties were obtained from the Aluminum Association [12].

Table 2: Summary of isotropic linear elastic material properties used in FEM model.

Component	Material	$\boldsymbol{E}$, lb/in^2	$\boldsymbol{\nu}$
Pin	Steel	30E6	0.3
Stiffener	Al 7178	10.2E6	0.33
Skin	Al 7075	10.3E6	0.33

Again it was useful to have each FEM component in its own separate group as this made selection of all the appropriate elements far more simple.

2.4.2 Thermal Properties

One additional isotropic property was defined in order to simulate the interference fit (Load Case 0). The elements which made up the straight shank portion of the pin were assigned α_T=130E-6 / °F. This combined with the ΔT=100°F boundary condition discussed in Section 2.3.2 would simulate the 0.004 in diametric interference between the pin and its surrounding hole. Stress as a result of this interference was transferred to the hole's surface via the contact slide lines. In the analysis cases where the interference fit was not desired the ΔT=100°F boundary condition was simply removed and the presence of the α_T=130E-6 / °F material property would have not impact on the model.

2.4.3 Gap Elements

By far the most complex portion of property assignment involved the gap elements. As stated earlier many of the available property assignments in the MSC/NASTRAN gap element do not produce convergent solutions. Other, per the recommendation of the MSC application engineers, need to be set within specific bounds to obtain a successful analysis result. The following values are the result of a significant period of trial and error by the author and several MSC engineers. Explanation is offered wherever relevant.

Per the MSC/NSATRAN guide, gap element between coincident nodes must have a gap orientation coordinate system defined to distinguish the closing direction from the opening direction. Specifically, the gap orientation coordinate system must have the +x-axis running from the "GA nodes" contact surface to the "GB node" contact surface. The directions of the y and z axis are not important. Recall that closing a gap element is synonymous with contact while opening is no contact. The MSC/PATRAN Geometry tool makes creating this coordinate system straight forward. As shown in Figure 7, the GA nodes were on the stiffener and the GB nodes were on the skin. Therefore the gap orientation axis system is defined with the +x-axis in the same direction as the +z-axis of the model's global coordinate system. The coordinate system is identified in the CID field of the MSC/NASTRAN "CGAP" cards. These are the same cards which define the GA and GB node pairs. All other properties are found in the MSC/NASTRAN "PGAP" card in the field specified in the parenthesis as follows. The axial stiffness for a closed gap (***KA***) was 1E10 lb/in^2. ***KA*** is the value of stiffness used to transfer a contacting load from one material to the other. While it might be tempting to assign a far higher value owing to the nearly infinite stiffness nature of contact—higher values led to divergent solutions. Arguably, a stiffness of 3 to 4 orders of magnitude higher than the surrounding material can be considered acceptably high and in fact is precisely what MSC recommends [7]. The axial stiffness for an open gap (***KB***) was 10 lb/in^2. ***KB*** is the value of stiffness used between nodes when there is no contact. Here again, one might be tempted to assign a value of zero to the case of no contact. Having zero stiffness assigned to a 1D bar element produces singularities in the solution that also tend to create divergent solutions. This requirement was not hard to live with since from an analysis point of view, ***KB***=10 lb/in^2 is nearly zero. The last property specified was the maximum allowable penetration (***TMAX***). As the name implies, this property defined the amount one contacting surface was permitted to penetrate the other during iteration steps. While the

engineer may deem zero to be the appropriate value here, this too caused problems with solution convergence. ***TMAX***=0.001 in was the minimum acceptable value that would permit the model's solution to converge. All other values were left in their default setting. As previously mentioned, any attempt to assign sliding friction or transverse stiffness properties led to model divergence.

2.5 Analysis

The FEM model analysis chosen for the present work were the two analysis cases requested by the CESI corrosion kinetic team. These were the Hi-Lok preload (Load Case 1) with and without the Hi-Lok pin interference fit (Load Case 0). All analysis was done by nonlinear static MSC/NASTRAN solution sequence 106. Several solution parameters were chosen to make convergence possible and are described in the following paragraph. Solution sequence (solver) 106 breaks the load in each Load Case up into a finite number of uniform load increments. The solver will iterate on each of these increments a defined number of times in an attempt to achieve convergence. If convergence is not achieved in this number, the load increment will be divided in half and the iteration process will repeat. Load increment division continues until convergence is obtained or an assigned maximum load division number is reached. As convergence is obtained the solver moves to the next load increment until 100% of the load for that Load Case is reached. The solver then moves on to subsequent Load Cases in the order they were assigned until the last one is reached. Each of the solver parameters mentioned are defined on of the sub-menus in the MSC/PATRAN ***Analysis*** tool. MSC/PATRAN then assigned these to the appropriate MSC/NASTRAN control cards when creating the analysis deck. Finally, two of the convergence criteria tolerances needed to be assigned slightly larger values than the default values found in MSC/PATRAN 2003. The "Load Error" and "Work Error" convergence criteria were change to the values found in earlier software versions. These like all the above changes from the default were per MSC engineers who felt they led to more stable solutions. Table 3 summarizes the values used to achieved a convergent solution and applicable the MSC/PATRAN sub-menu. The parameter name is as used in those sub-menus.

Table 3: Summary of key MSC/PATRAN *Analysis* parameter assignments required for FEM model convergence.

Parameter Name	**MSC/PATRAN *Analysis* sub-menu**	**Value**
Large Displacements	Solution Parameters	YES
Follower Forces	Solution Parameters	YES
Number of Load Increments	Subcase Parameters	10
Matrix Update Method	Subcase Parameters	Controlled Iteration
Number of Iterations per Update	Subcase Parameters	5
Allowable Iteration per Increment	Subcase Parameters	8
Convergence Criteria: Load Error	Subcase Parameters	0.1
Convergence Criteria: Work Error	Subcase Parameters	0.1

3. Results

The results for the two cases are shown graphically in the figures that follow. The MSC/PATRAN post-processing ***Results*** tool was used to create graphical contour plots of the stress results requested by the CESI Corrosion Kinetics Team. Plots are for the skin component and are for the fastener near field. All figures are top view (looking in the –z direction) as oriented in Figure 1 with the exception of the bottom thickness plane which looking up (+z-axis direction). Plots were generated for the x, y, and z components of the stress tensor as well as hydrostatic stress. Each stress was plotted at five thickness planes. These were top plane (z=0), the ¼ t plane (z=−0.045 in), the ½ t plane (z=−0.090 in), the ¾ t plane (z=−0.135 in) and the bottom plane (z=−0.180 in). Figure 9 illustrates these result plane locations. For easy comparison, all contour plots use the same fringe color scale with the stress result being given in lb/in^2.

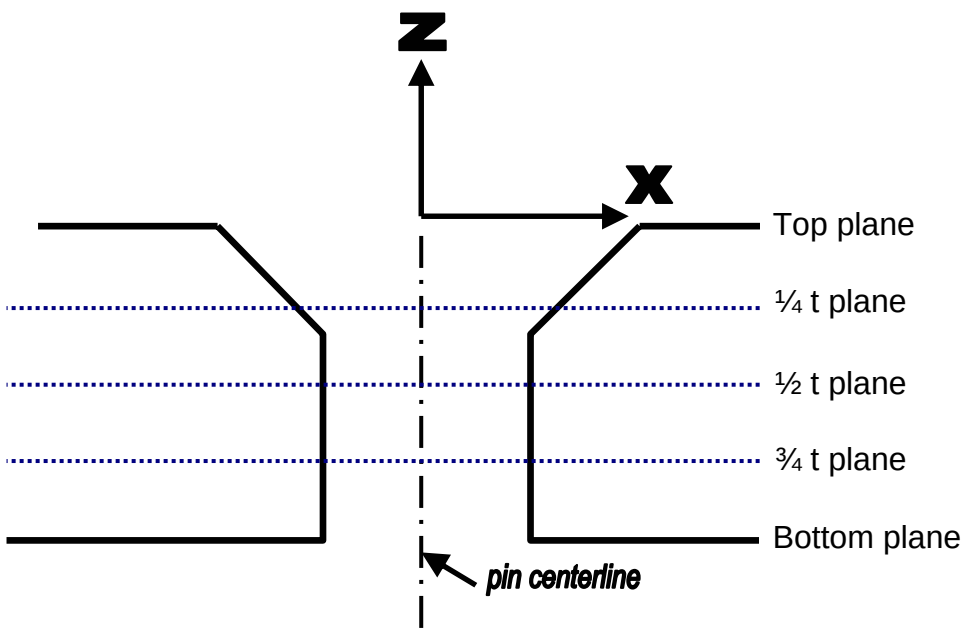

Figure 9: Thickness plane location of MSC/PATRAN *Results* stress fringe contour plots.

3.1 Result Case 1 – Hi-Lok Pre-Load with a Clean fit (no pin interference)

Figures 10 through 29 show the stress contour plots for this result case grouped first by thickness plane from top to bottom then by stress result in the following order; hydrostatic stress followed by the stress tensor x-component, y-component, z-component. The small axis in each figure is purely for orientation purposes and does not represent the global axis system.

3.2 Result Case 2 – Hi-Lok Pre-load with 0.004 in Diametric Interference Fit

Figures 30 through 49 show the stress contour plots for this result case with the same grouping as Section 3.1. Again the small axis in each figure is purely for orientation purposes and does not represent the global axis system.

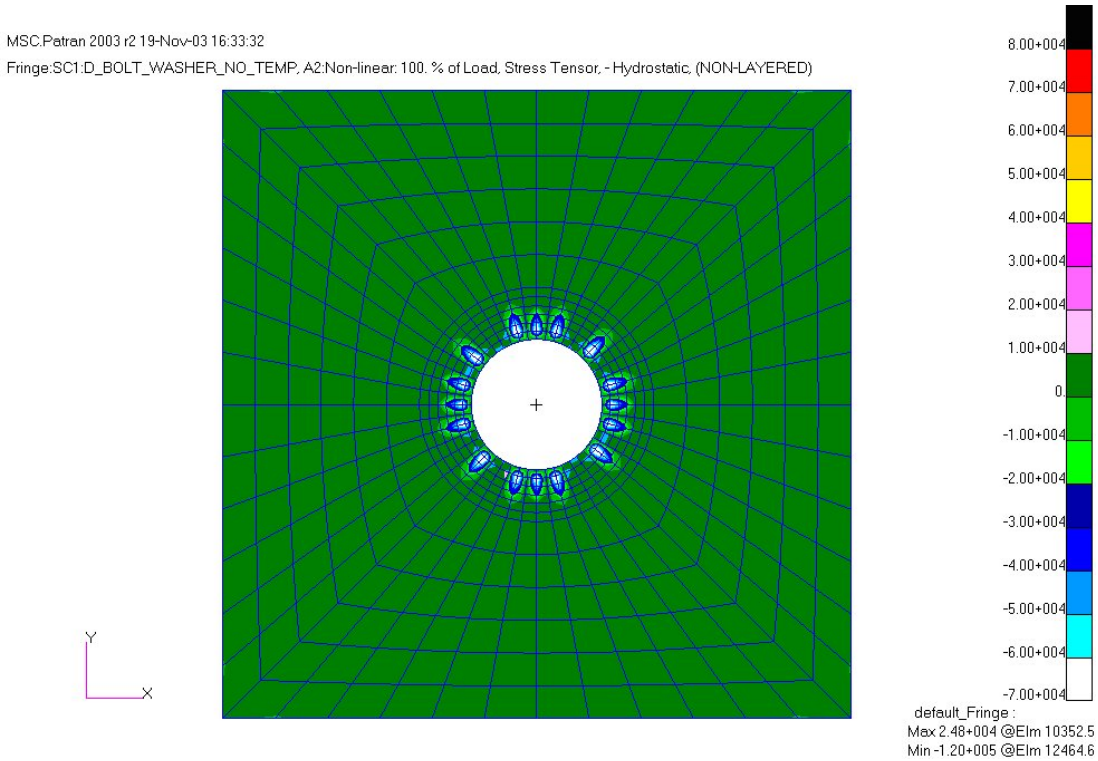

Figure 10: Hi-Lok pre-load with a clean fit, hydrostatic stress contour plot of top plane thickness location.

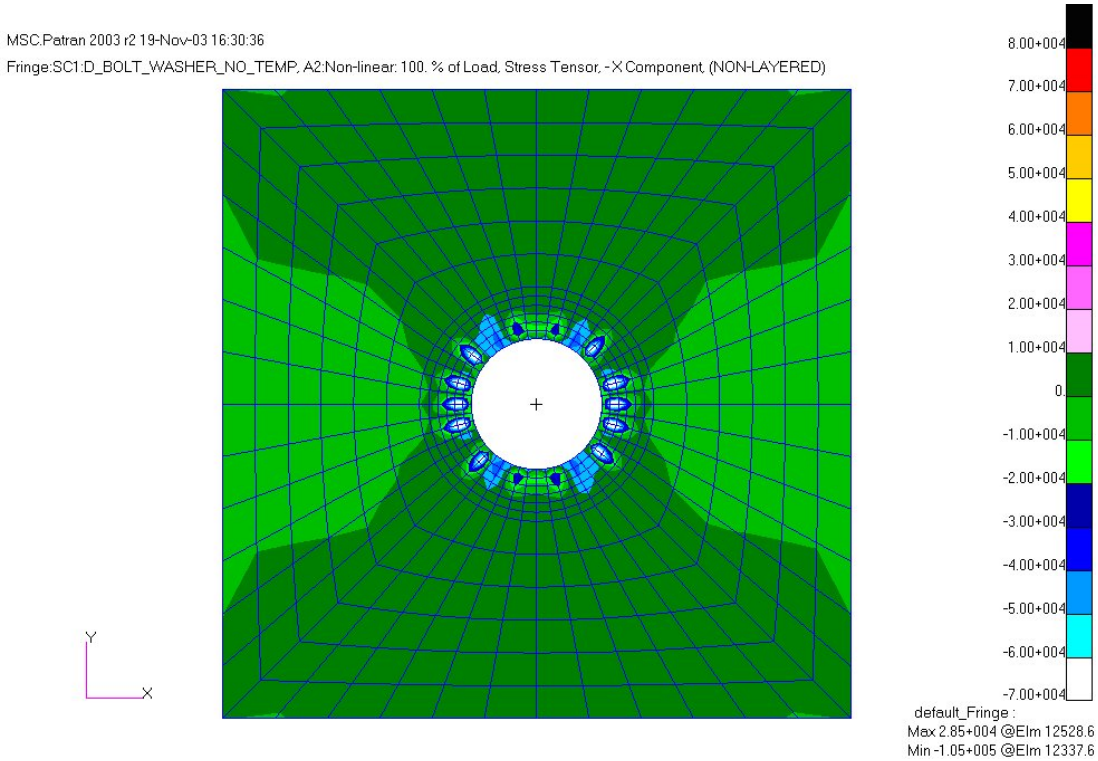

Figure 11: Hi-Lok pre-load with a clean fit, stress tensor x-component contour plot of top plane thickness location.

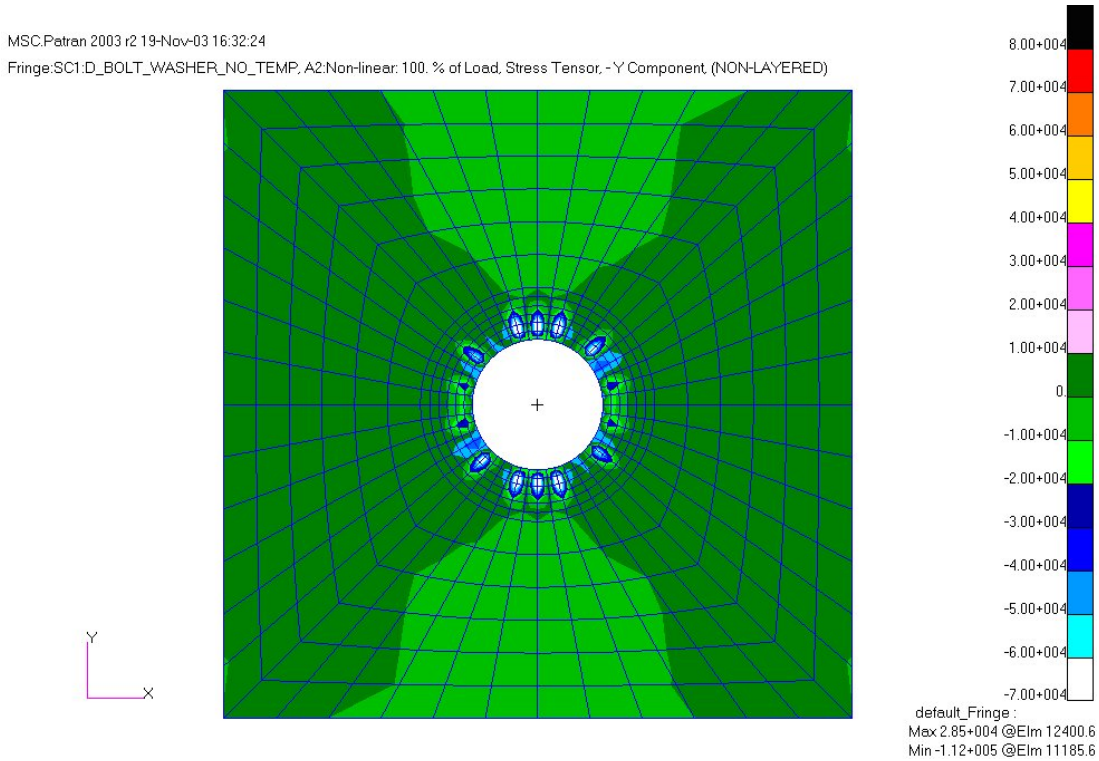

Figure 12: Hi-Lok pre-load with a clean fit, stress tensor y-component contour plot of top plane thickness location.

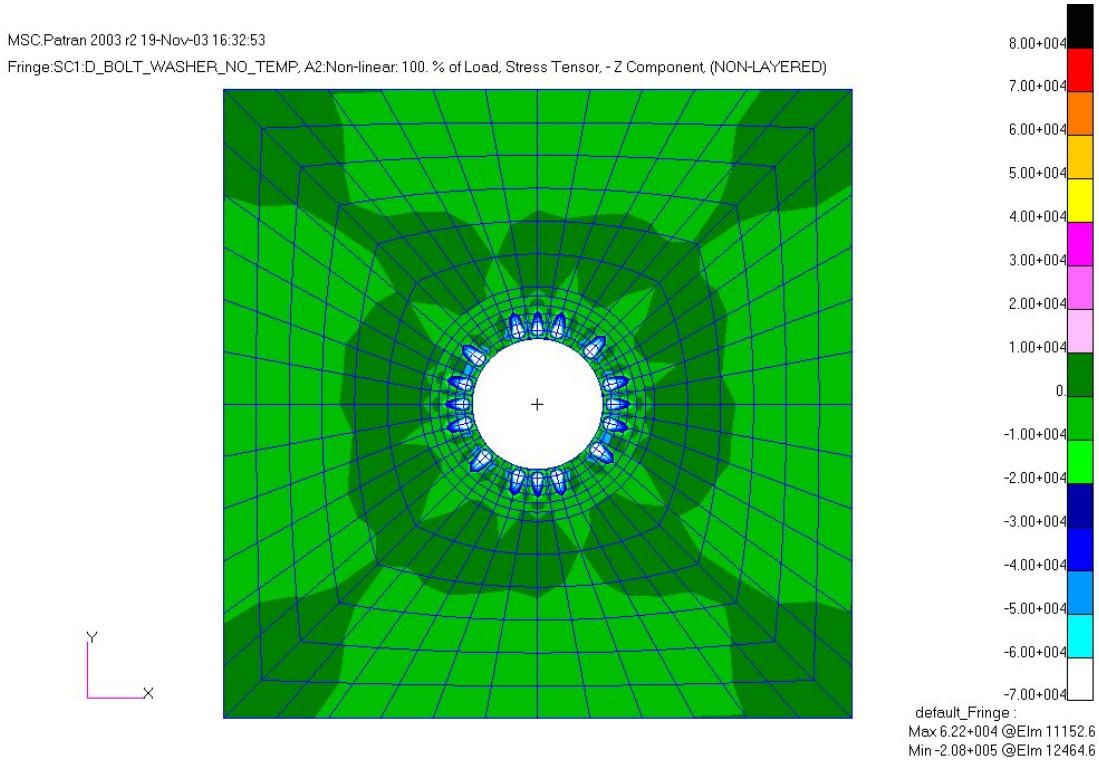

Figure 13: Hi-Lok pre-load with a clean fit, stress tensor z-component contour plot of top plane thickness location.

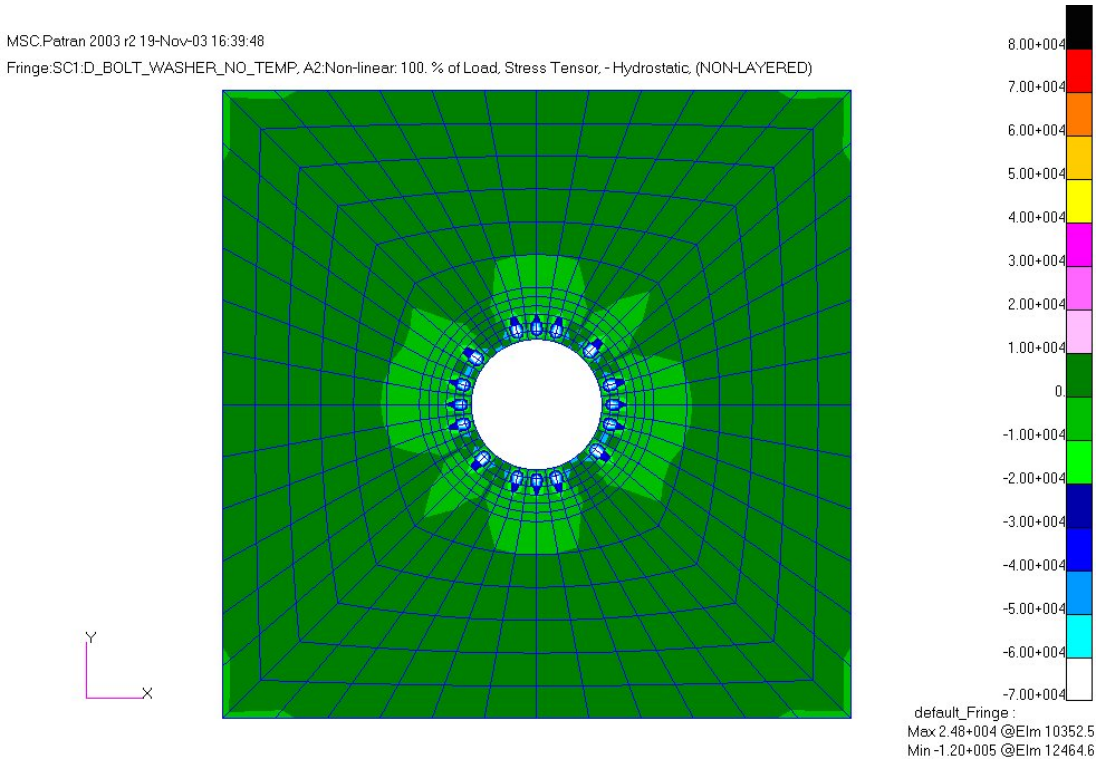

Figure 14: Hi-Lok pre-load with a clean fit, hydrostatic stress contour plot of ¼ t plane thickness location.

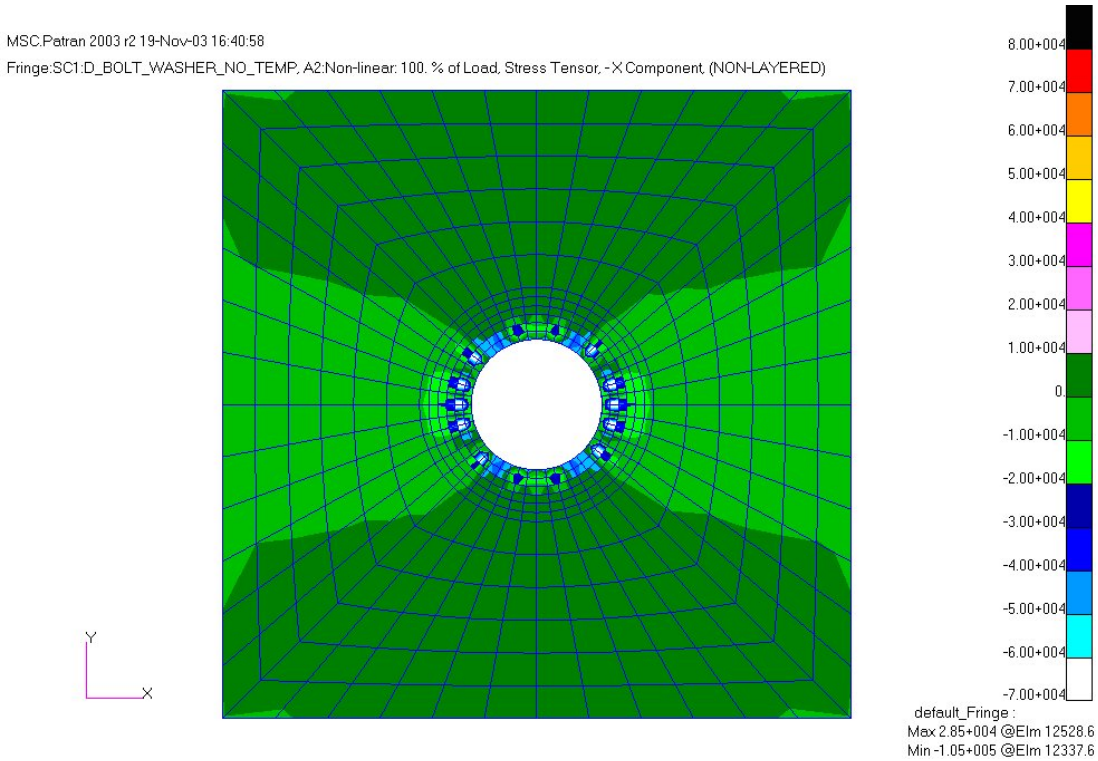

Figure 15: Hi-Lok pre-load with a clean fit, stress tensor x-component contour plot of ¼ t plane thickness location.

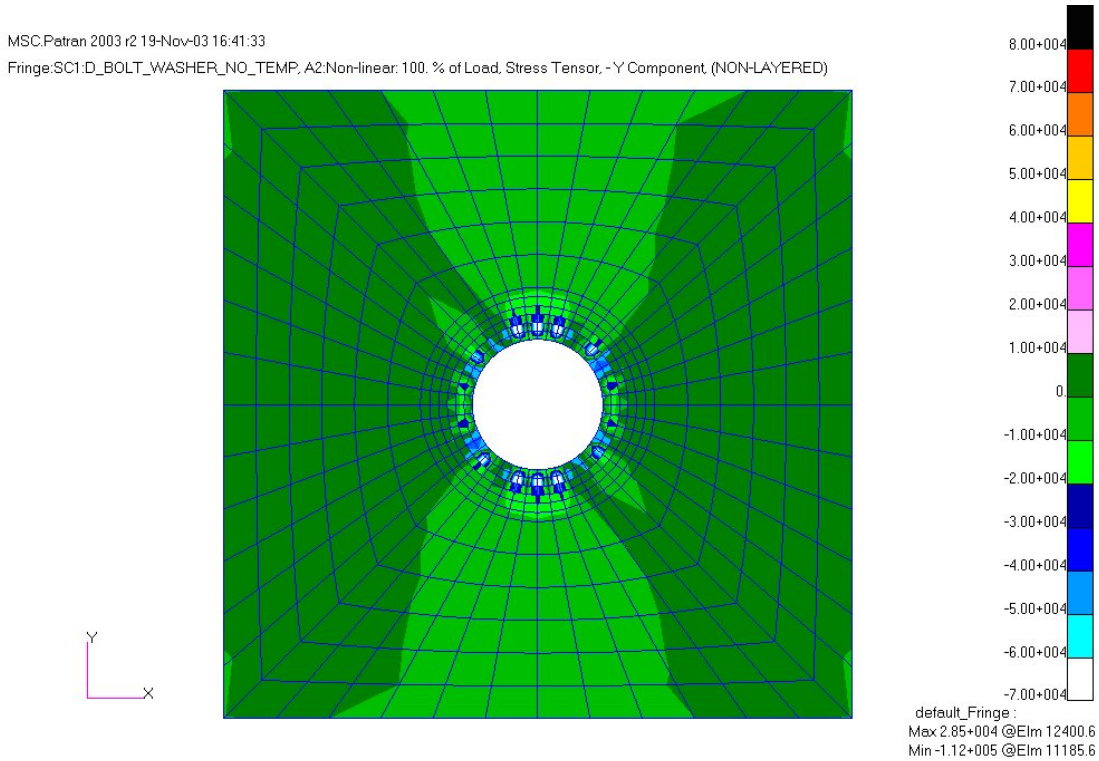

Figure 16: Hi-Lok pre-load with a clean fit, stress tensor y-component contour plot of ¼ t plane thickness location.

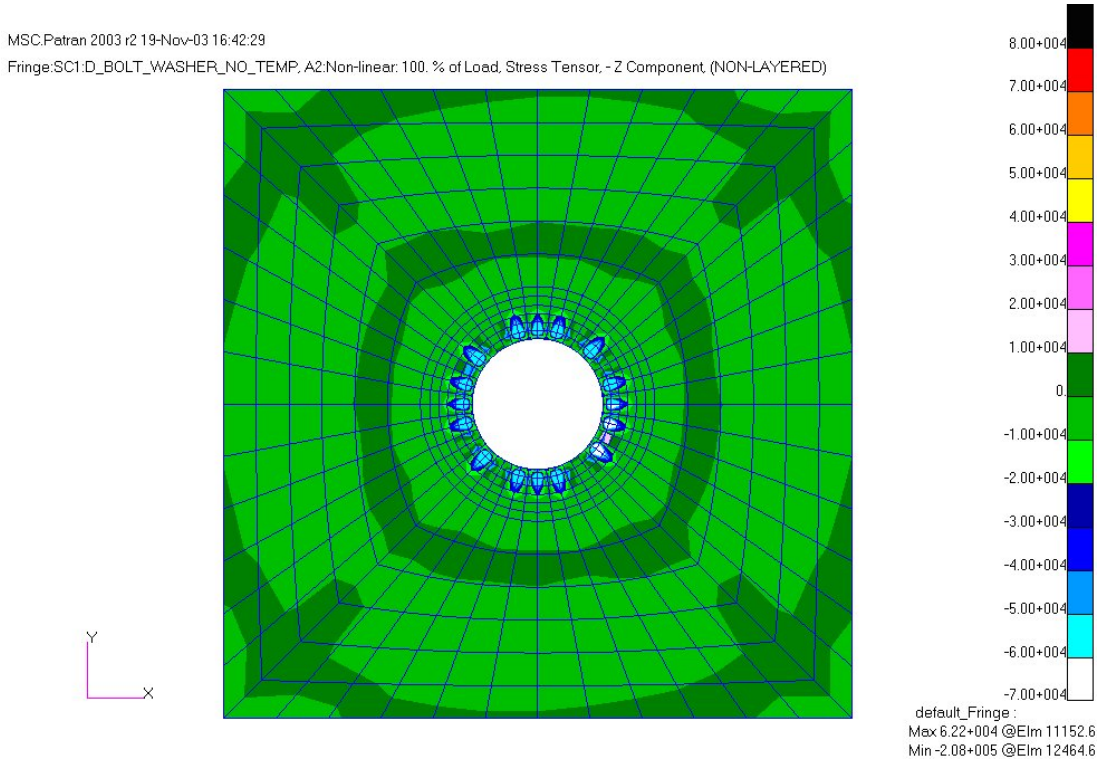

Figure 17: Hi-Lok pre-load with a clean fit, stress tensor z-component contour plot of ¼ t plane thickness location.

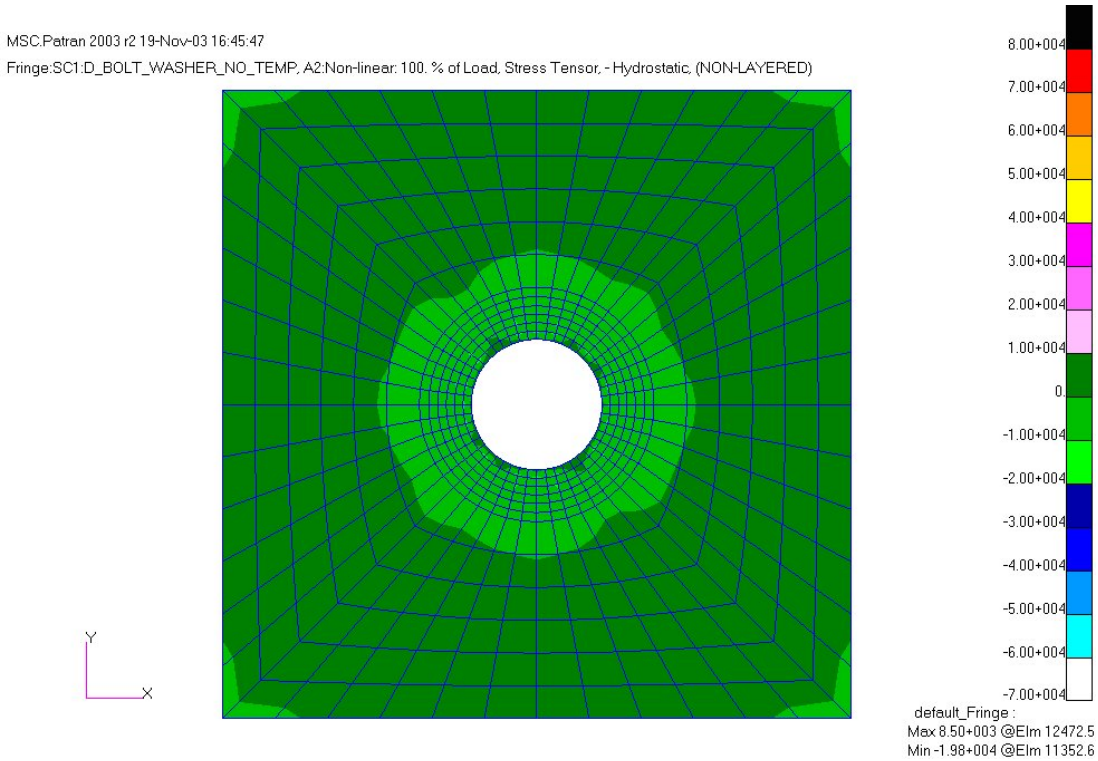

Figure 18: Hi-Lok pre-load with a clean fit, hydrostatic stress contour plot of ½ t plane thickness location.

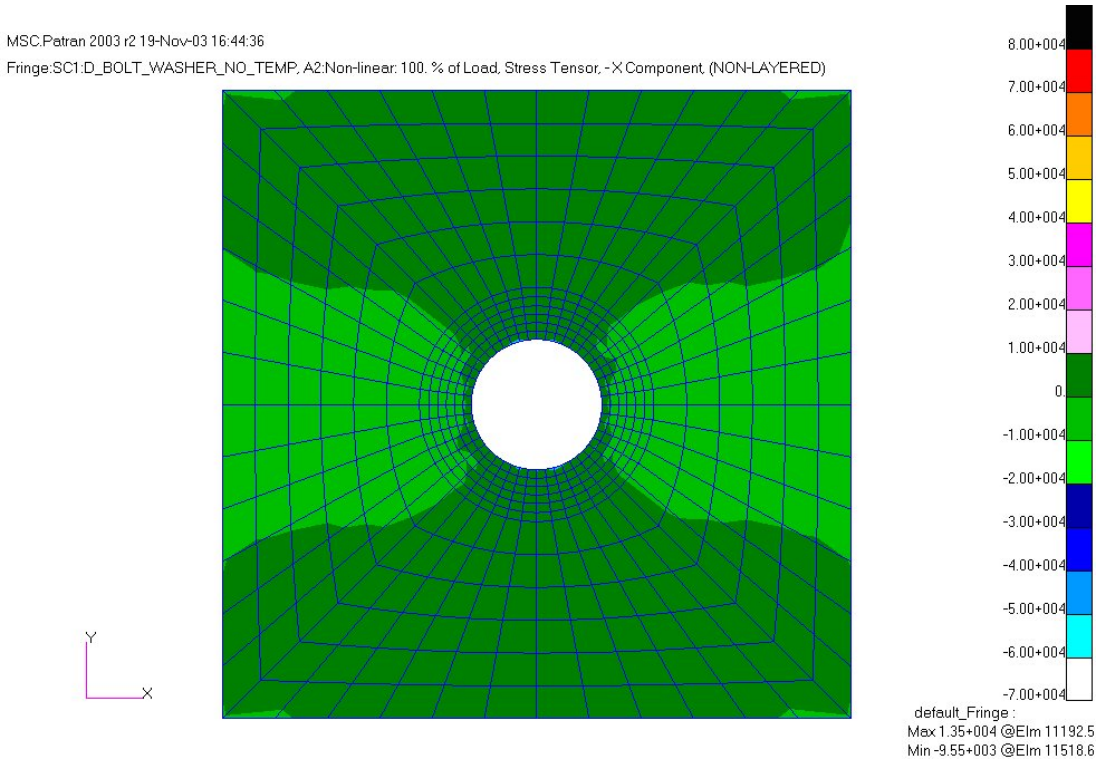

Figure 19: Hi-Lok pre-load with a clean fit, stress tensor x-component contour plot of ½ t plane thickness location.

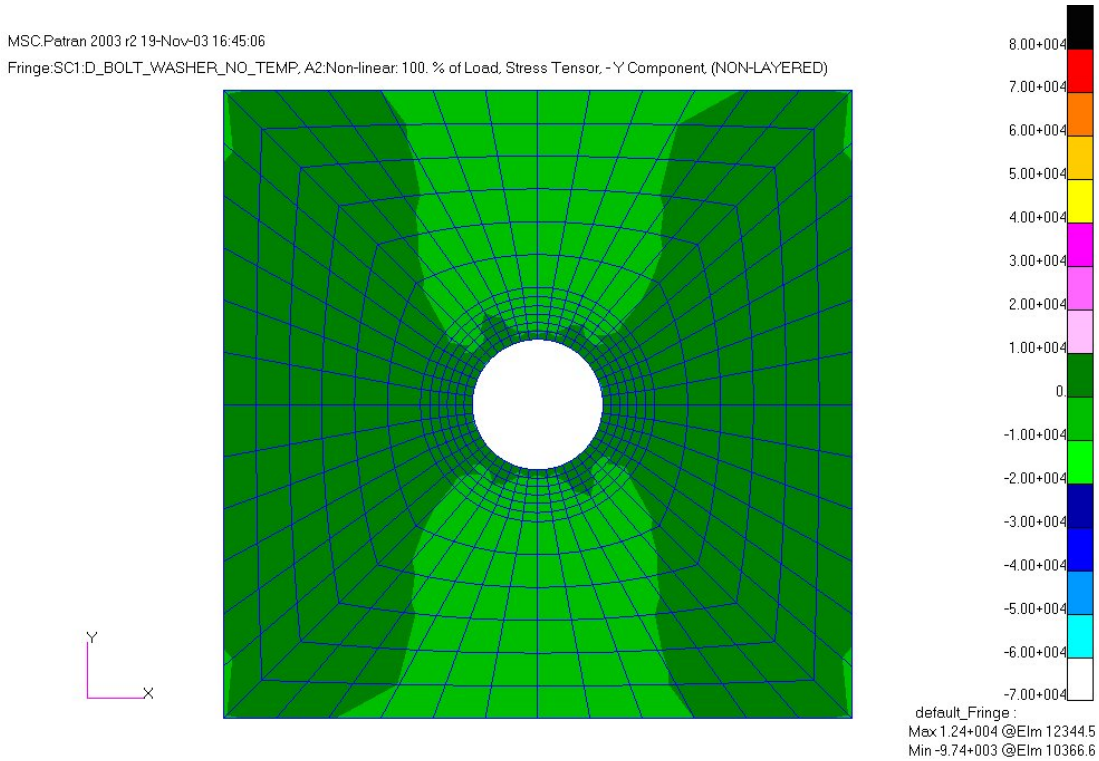

Figure 20: Hi-Lok pre-load with a clean fit, stress tensor y-component contour plot of ½ t plane thickness location.

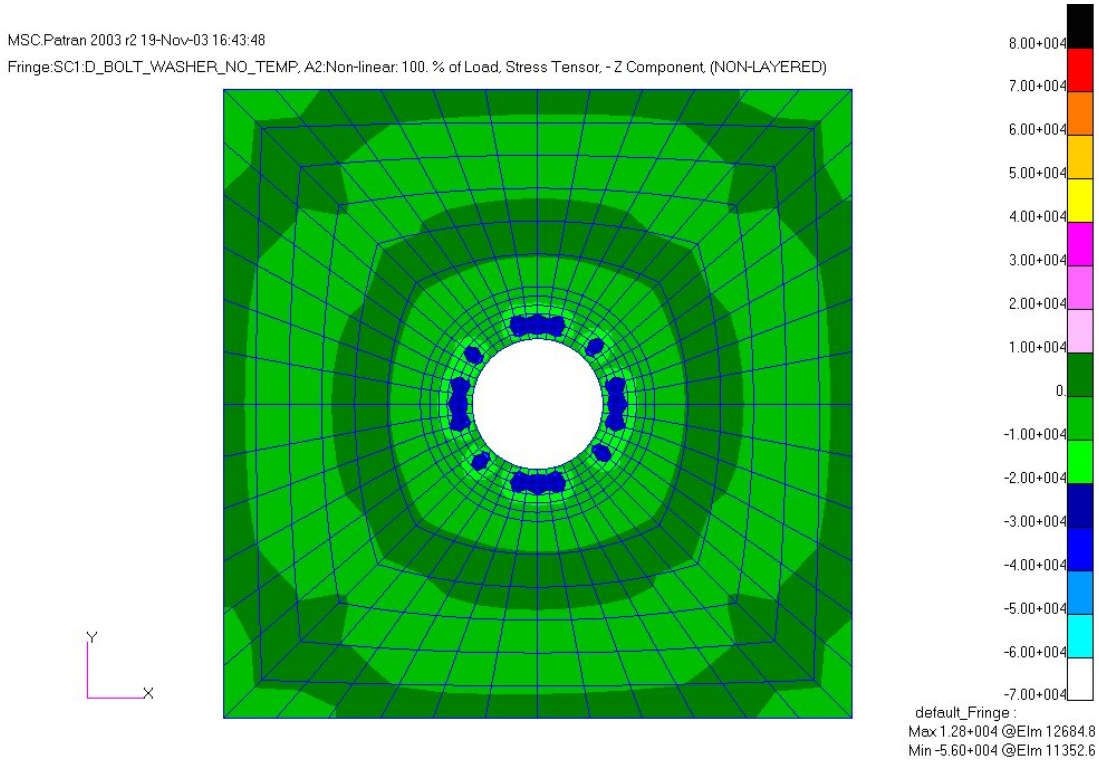

Figure 21: Hi-Lok pre-load with a clean fit, stress tensor z-component contour plot of ½ t plane thickness location.

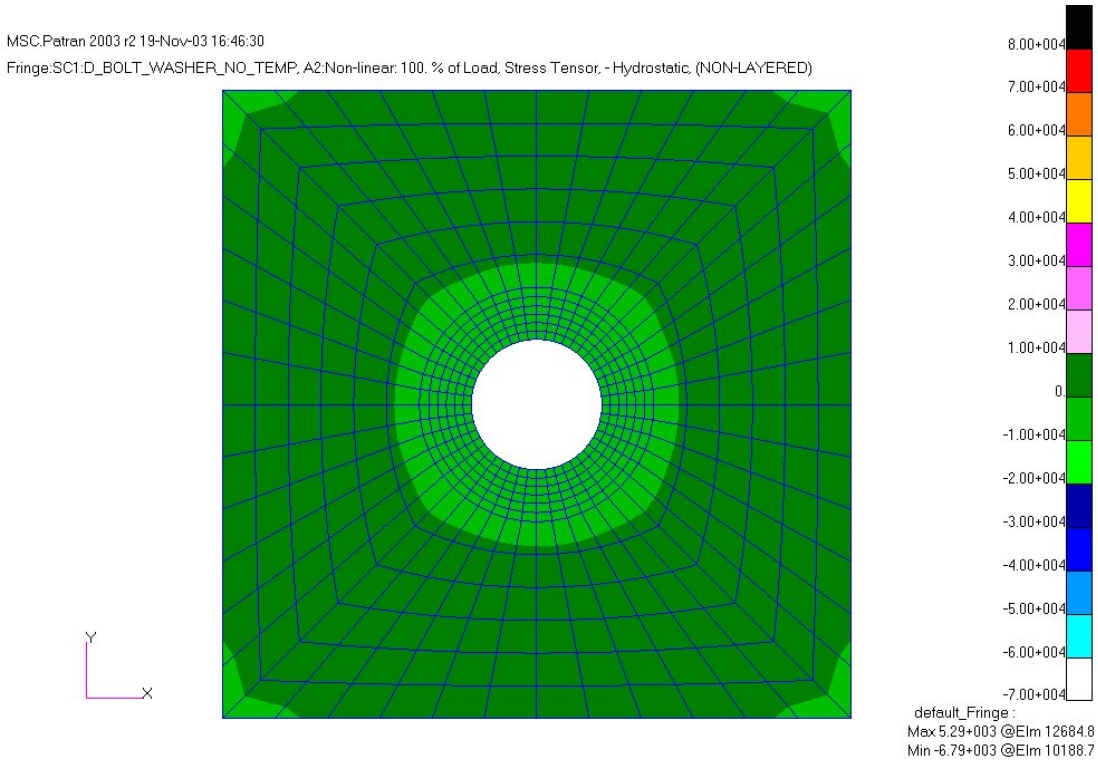

Figure 22: Hi-Lok pre-load with a clean fit, hydrostatic stress contour plot of ¾ t plane thickness location.

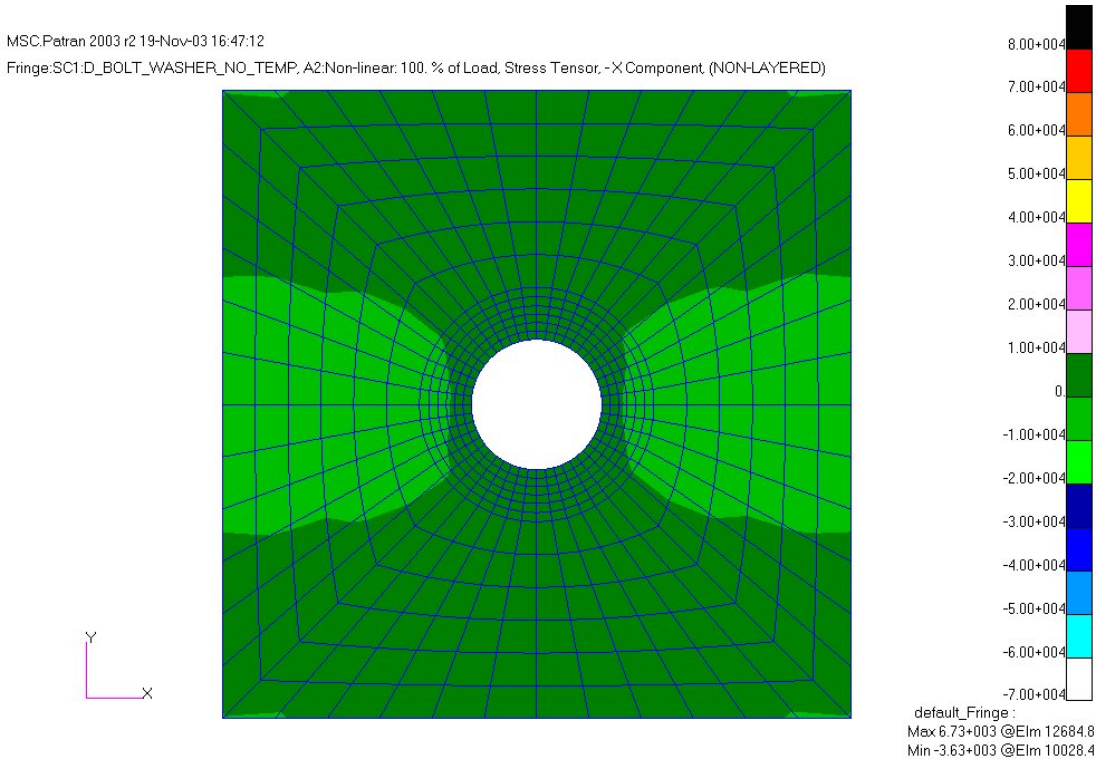

Figure 23: Hi-Lok pre-load with a clean fit, stress tensor x-component contour plot of ¾ t plane thickness location.

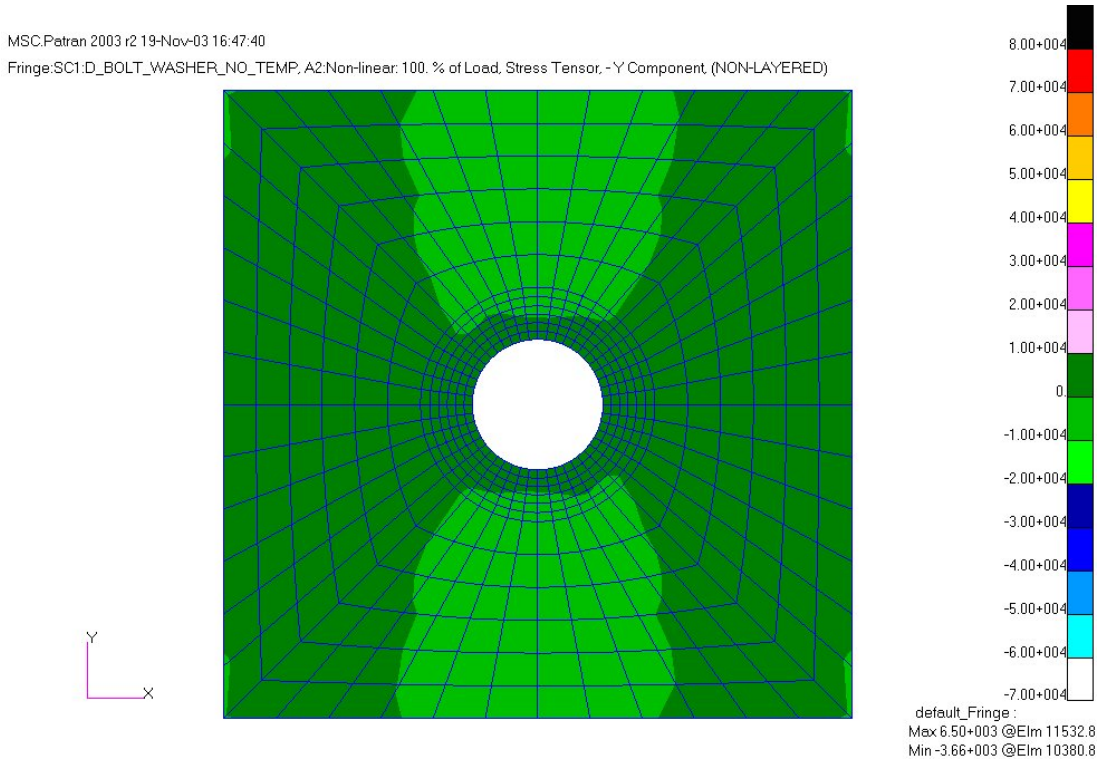

Figure 24: Hi-Lok pre-load with a clean fit, stress tensor y-component contour plot of ¾ t plane thickness location.

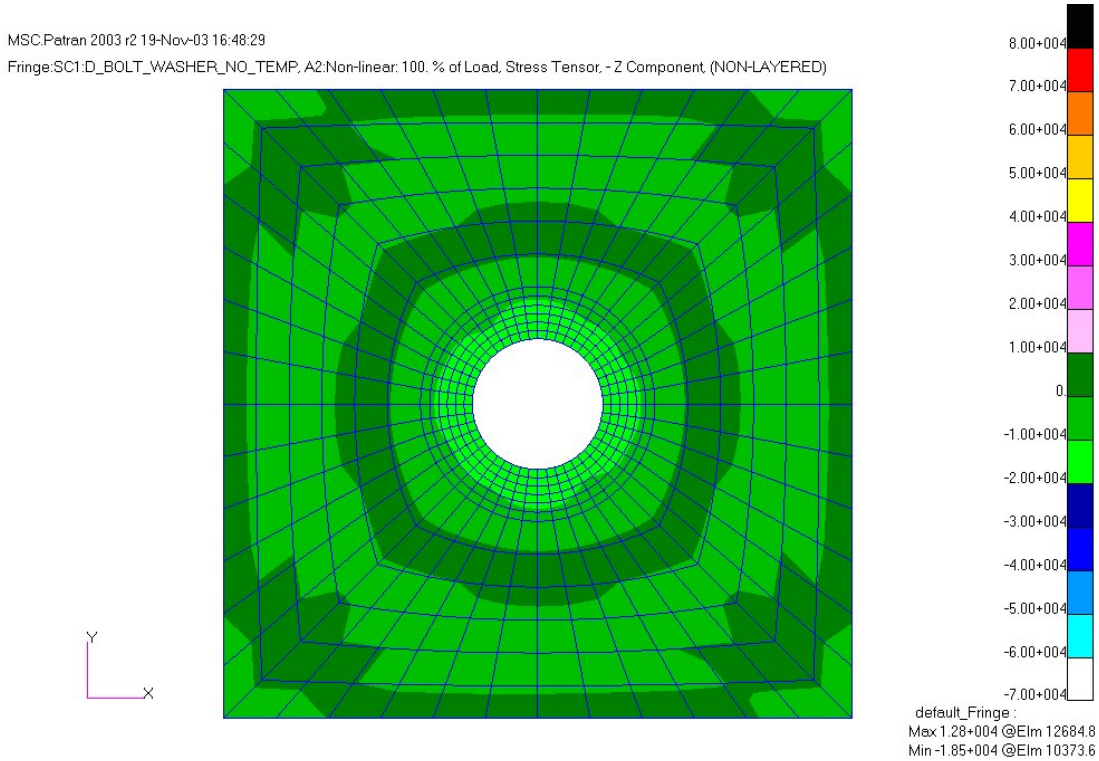

Figure 25: Hi-Lok pre-load with a clean fit, stress tensor z-component contour plot of ¾ t plane thickness location.

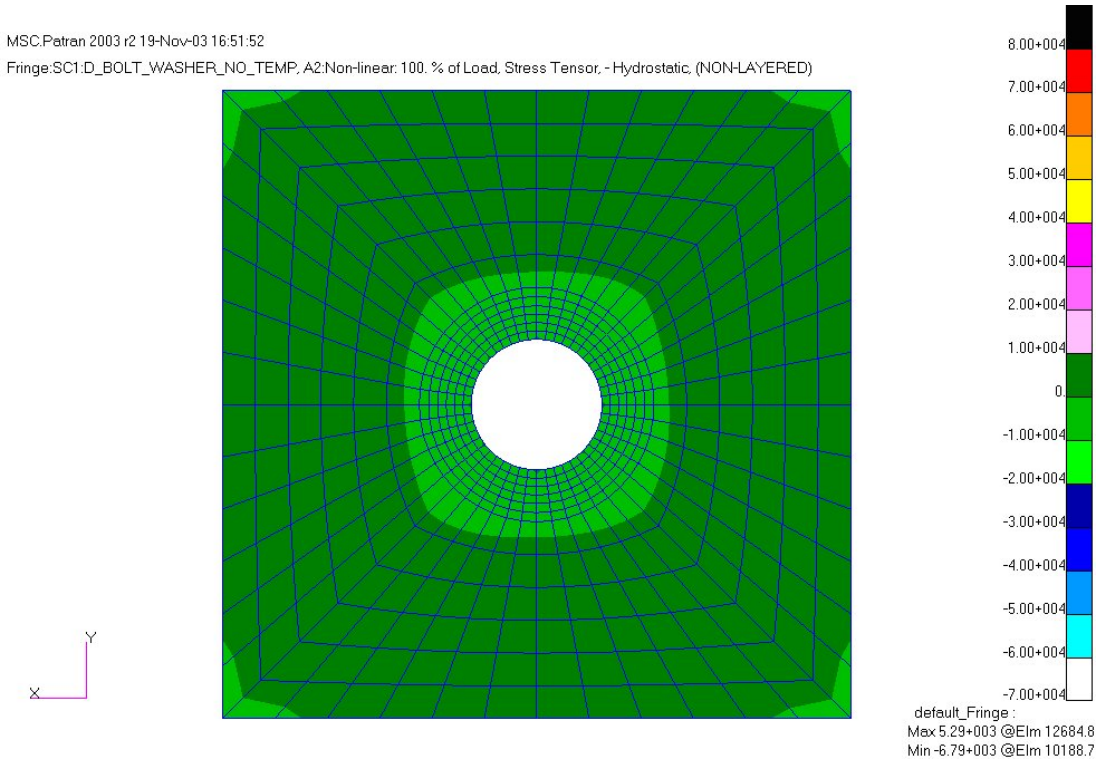

Figure 26: Hi-Lok pre-load with a clean fit, hydrostatic stress contour plot of bottom plane thickness location.

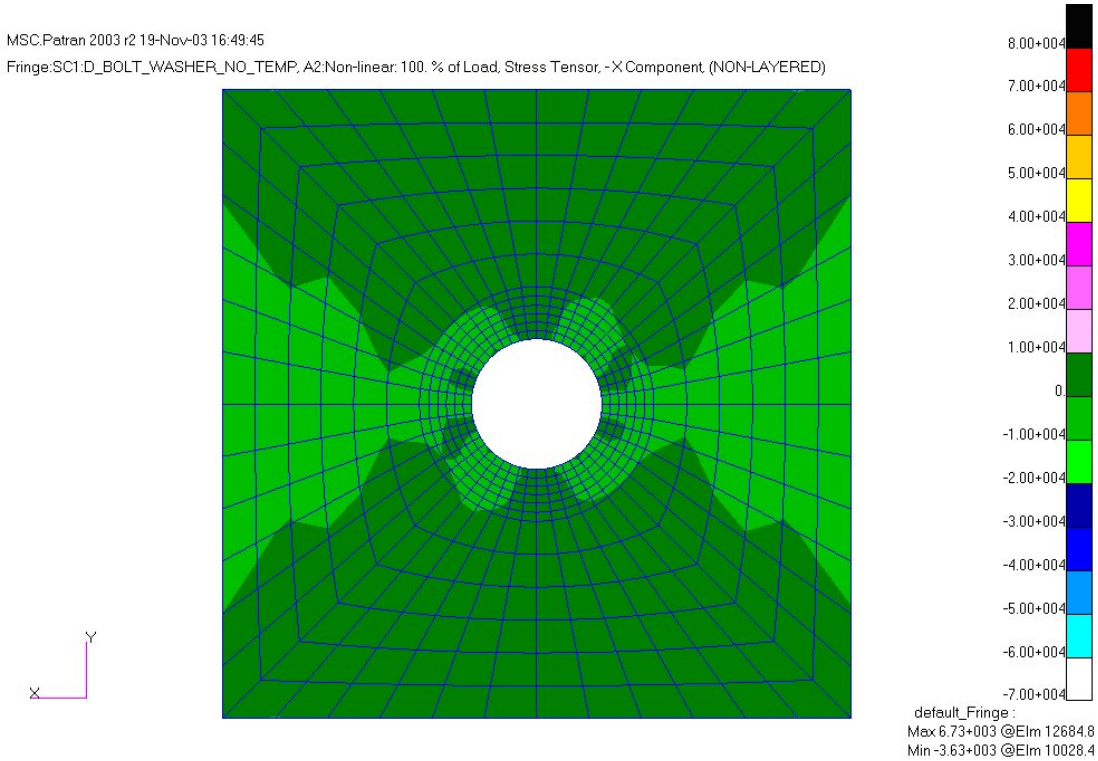

Figure 27: Hi-Lok pre-load with a clean fit, stress tensor x-component contour plot of bottom plane thickness location.

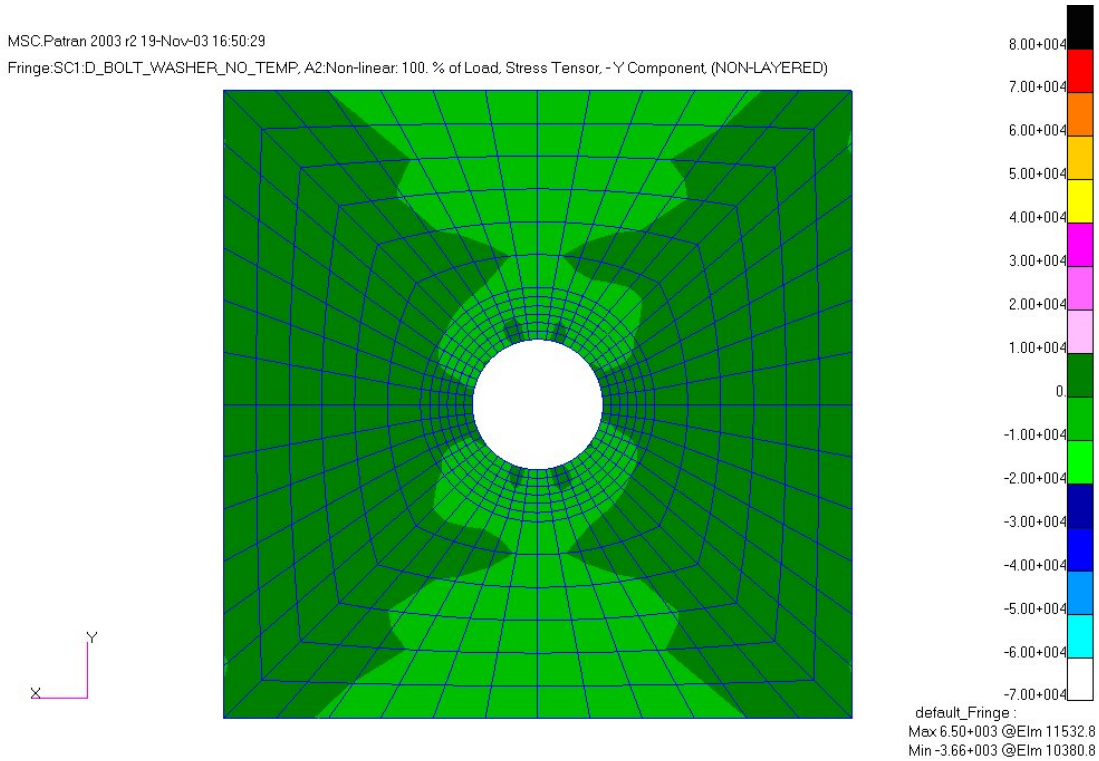

Figure 28: Hi-Lok pre-load with a clean fit, stress tensor y-component contour plot of bottom plane thickness location.

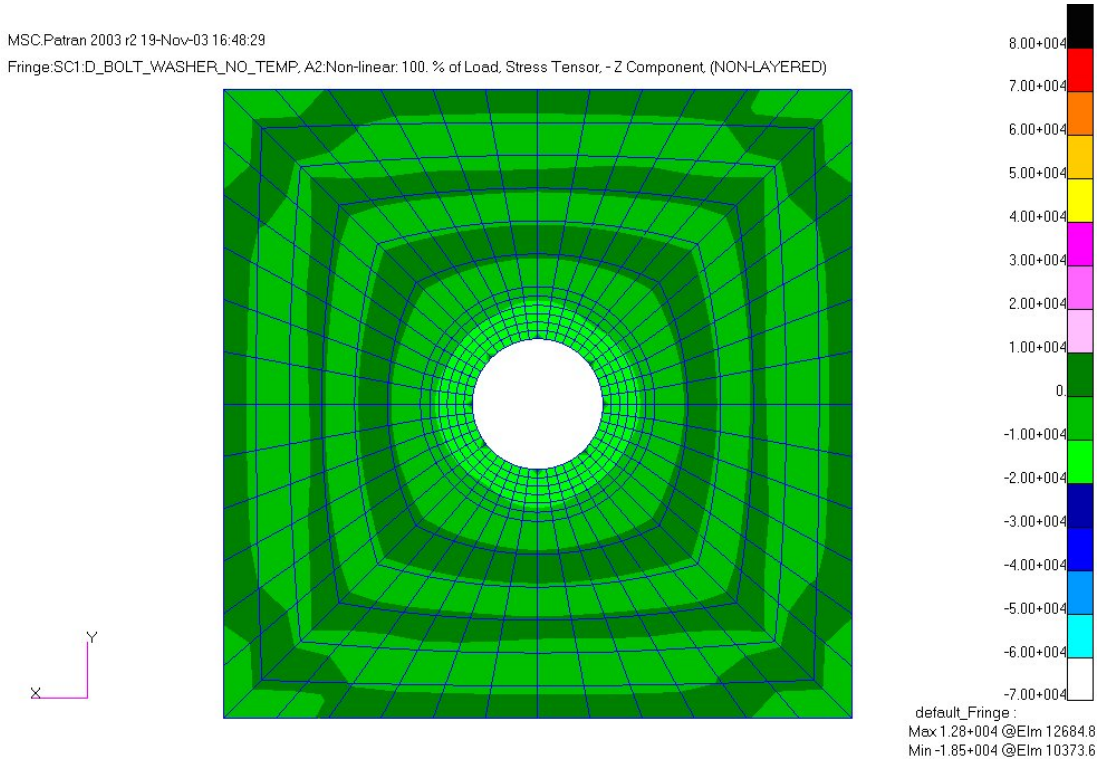

Figure 29: Hi-Lok pre-load with a clean fit, stress tensor z-component contour plot of bottom plane thickness location.

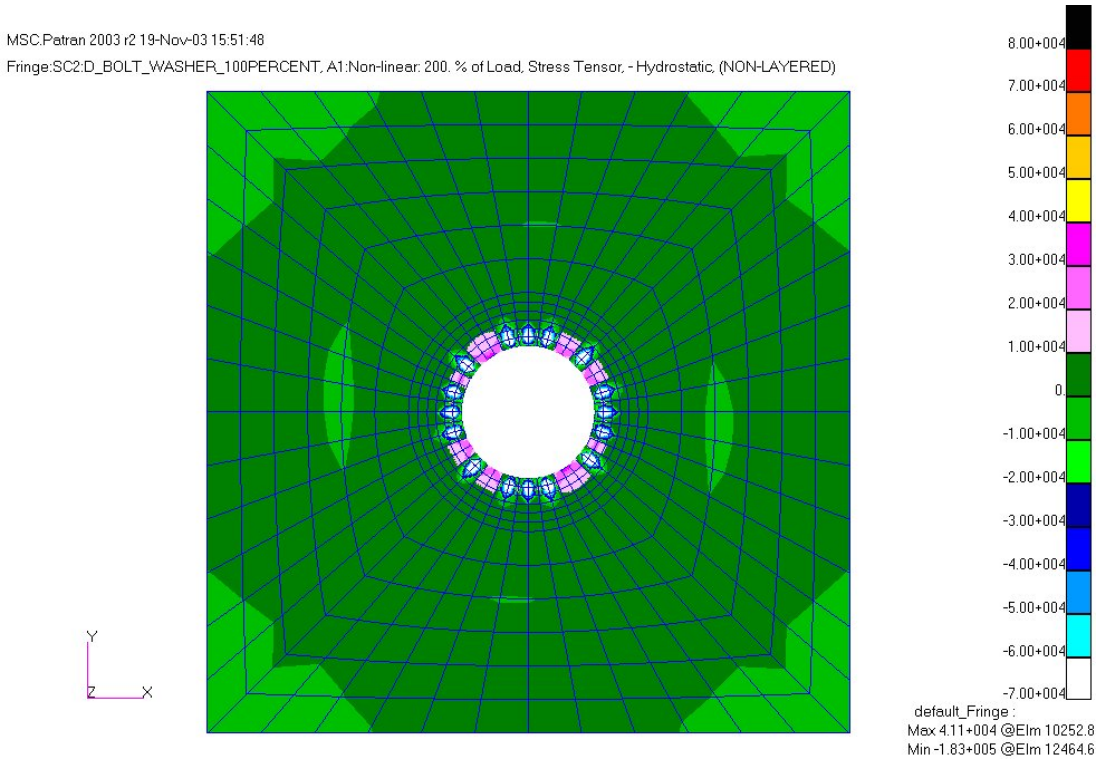

Figure 30: Hi-Lok pre-load with a 0.004 in interference fit, hydrostatic stress contour plot of top plane thickness location.

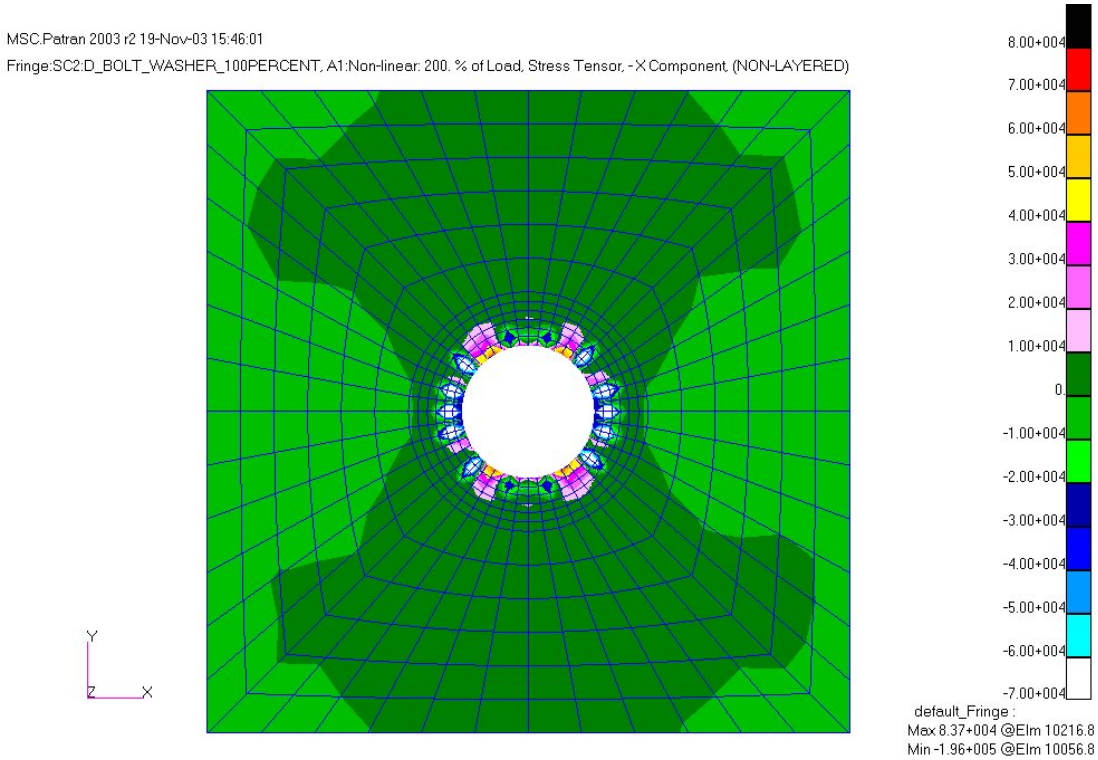

Figure 31: Hi-Lok pre-load with a 0.004 in interference fit, stress tensor x-component contour plot of top plane thickness location.

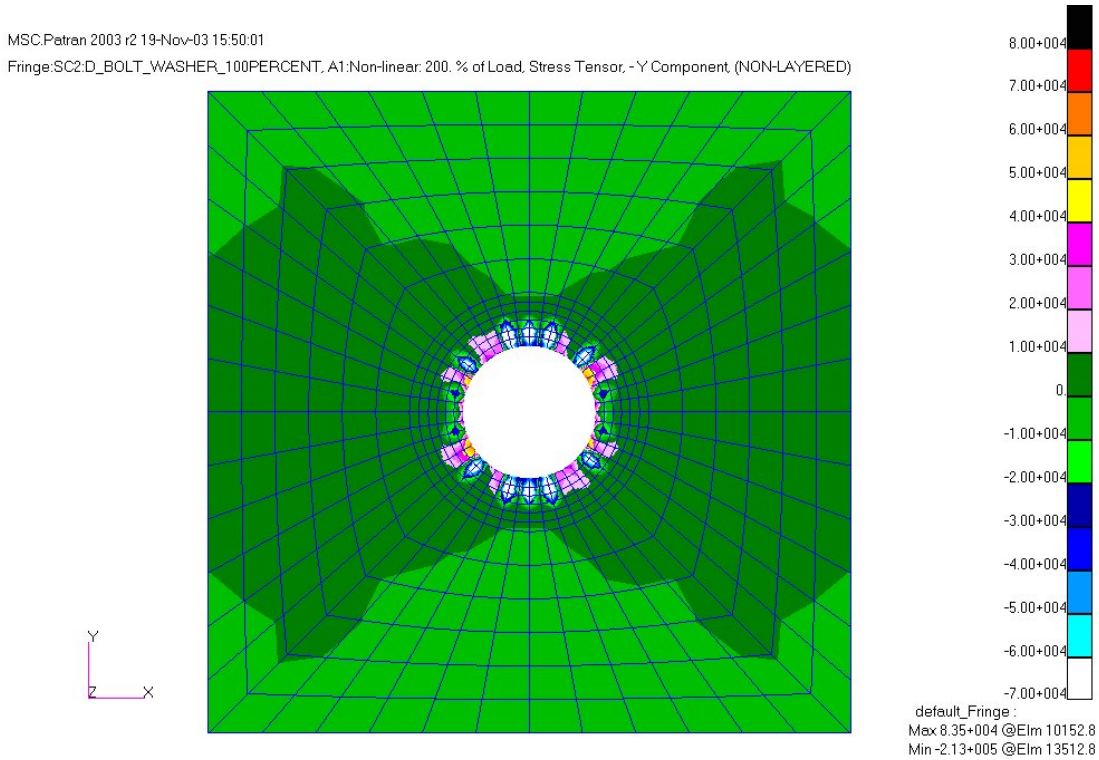

Figure 32: Hi-Lok pre-load with a 0.004 in interference fit, stress tensor y-component contour plot of top plane thickness location.

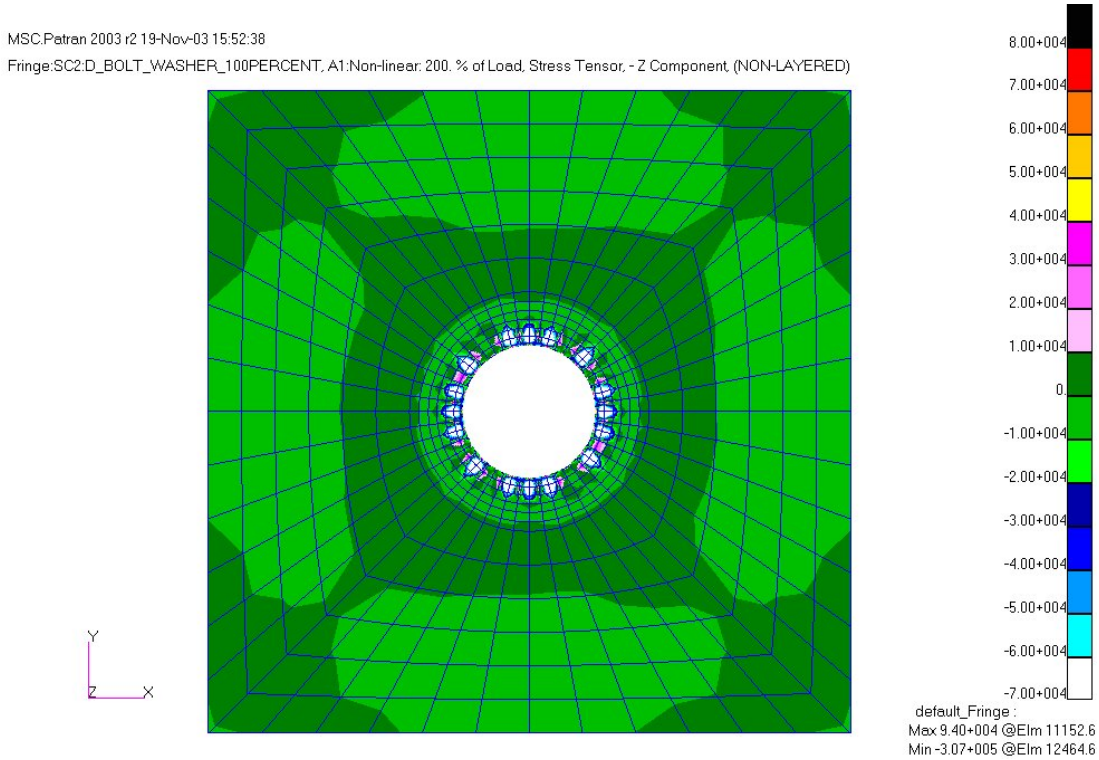

Figure 33: Hi-Lok pre-load with a 0.004 in interference fit, stress tensor z-component contour plot of top plane thickness location.

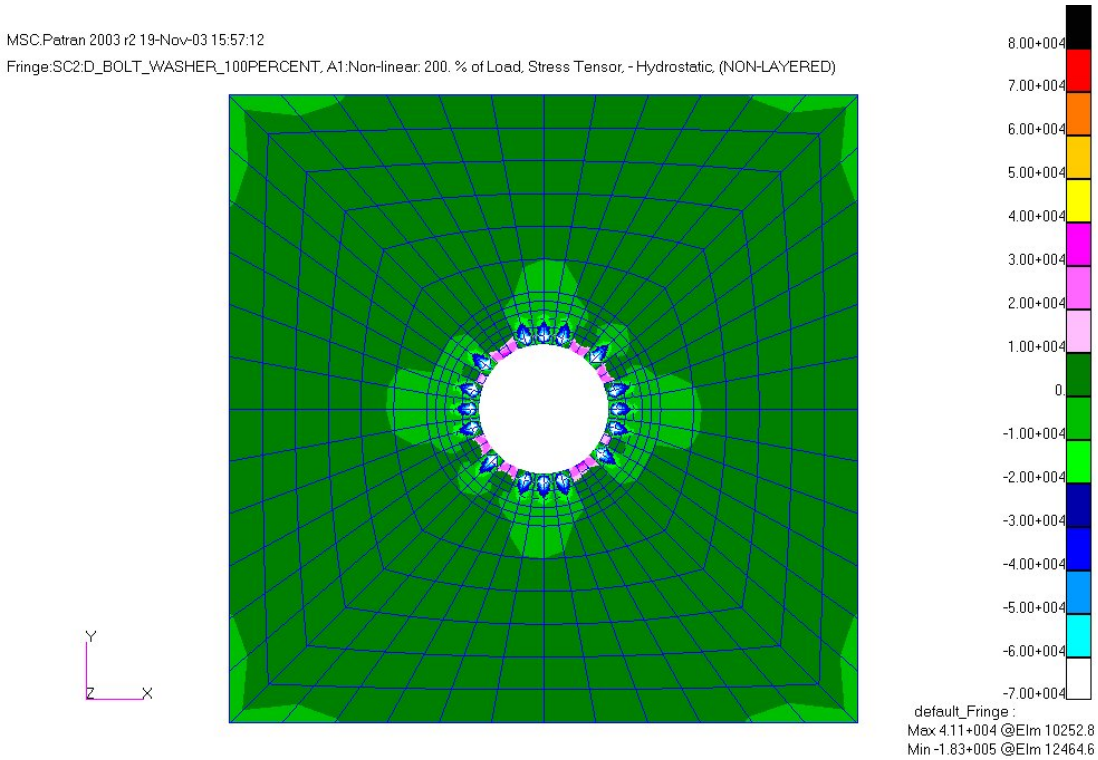

Figure 34: Hi-Lok pre-load with a 0.004 in interference fit, hydrostatic stress contour plot of ¼ t plane thickness location.

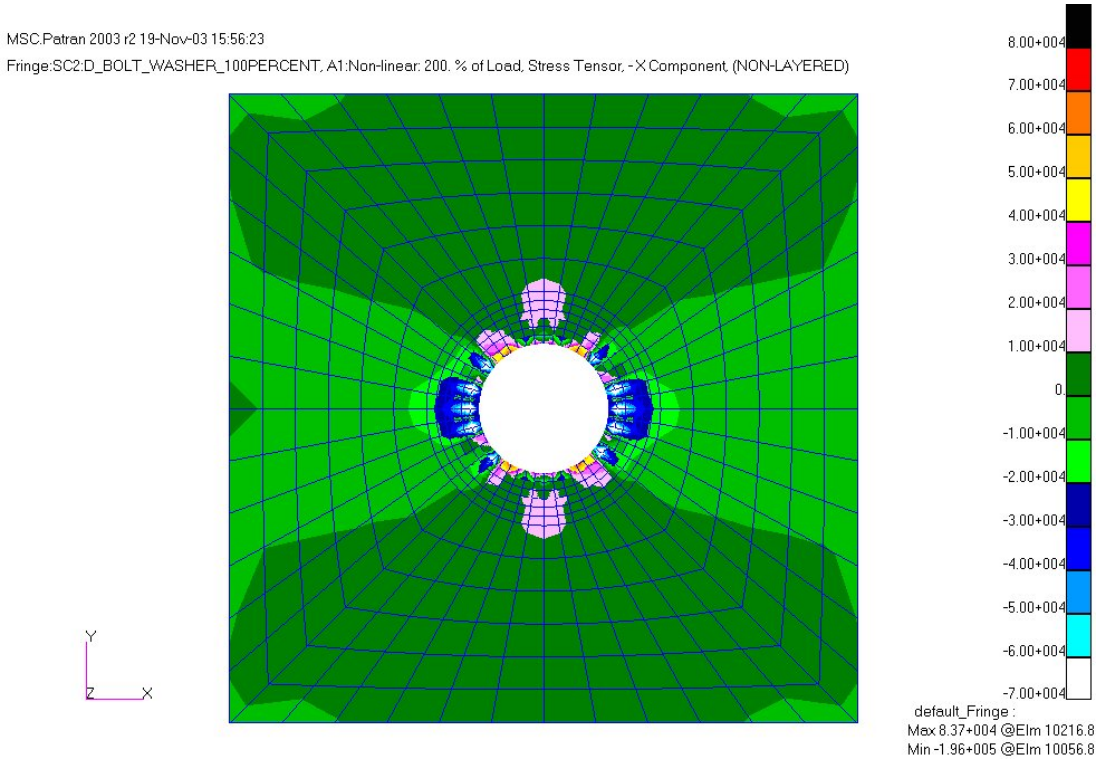

Figure 35: Hi-Lok pre-load with a 0.004 in interference fit, stress tensor x-component contour plot of ¼ t plane thickness location.

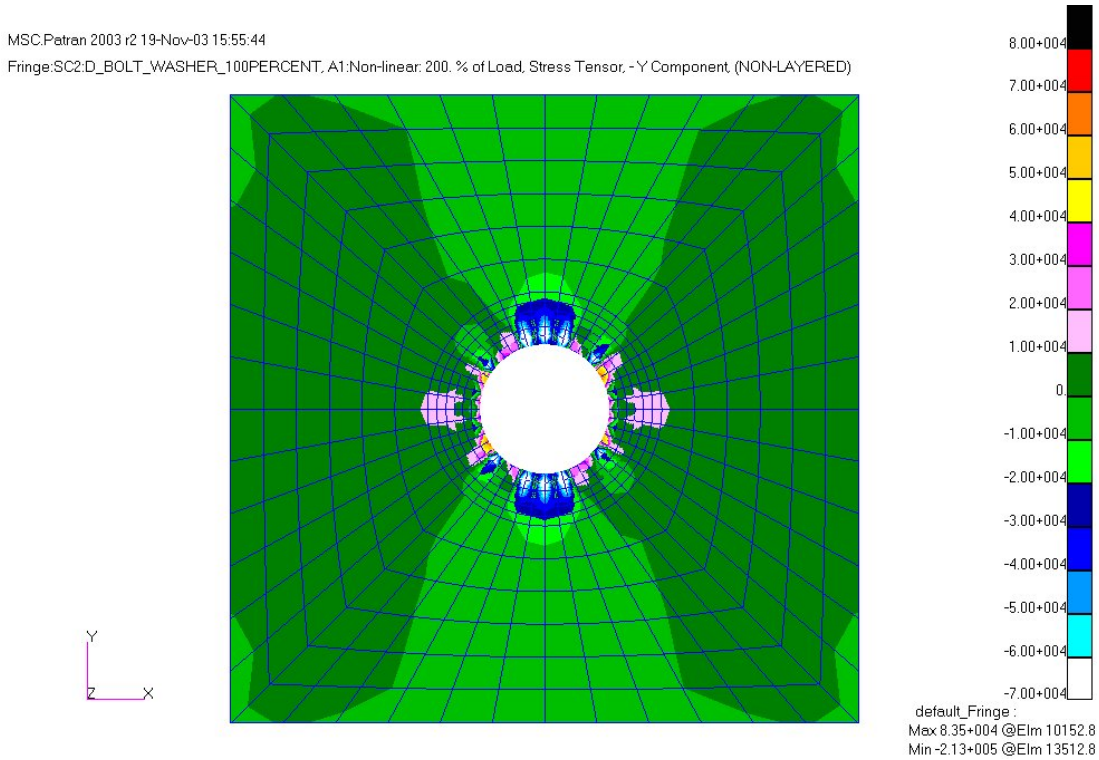

Figure 36: Hi-Lok pre-load with a 0.004 in interference fit, stress tensor y-component contour plot of ¼ t plane thickness location.

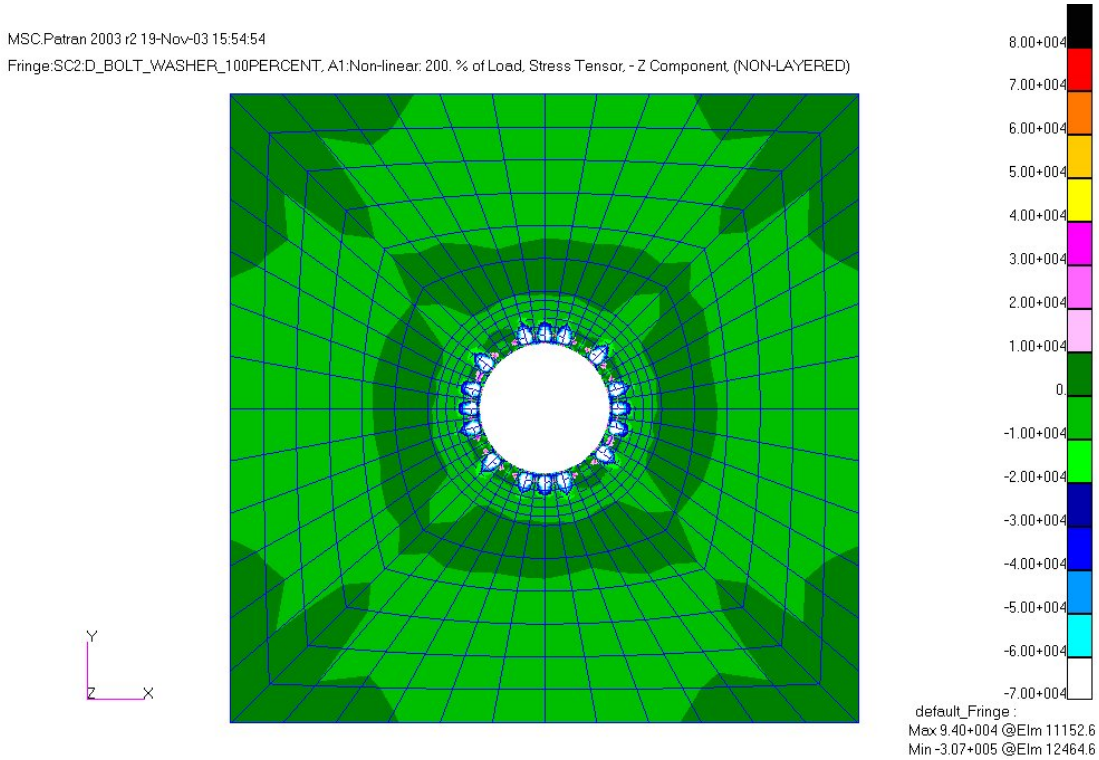

Figure 37: Hi-Lok pre-load with a 0.004 in interference fit, stress tensor z-component contour plot of ¼ t plane thickness location.

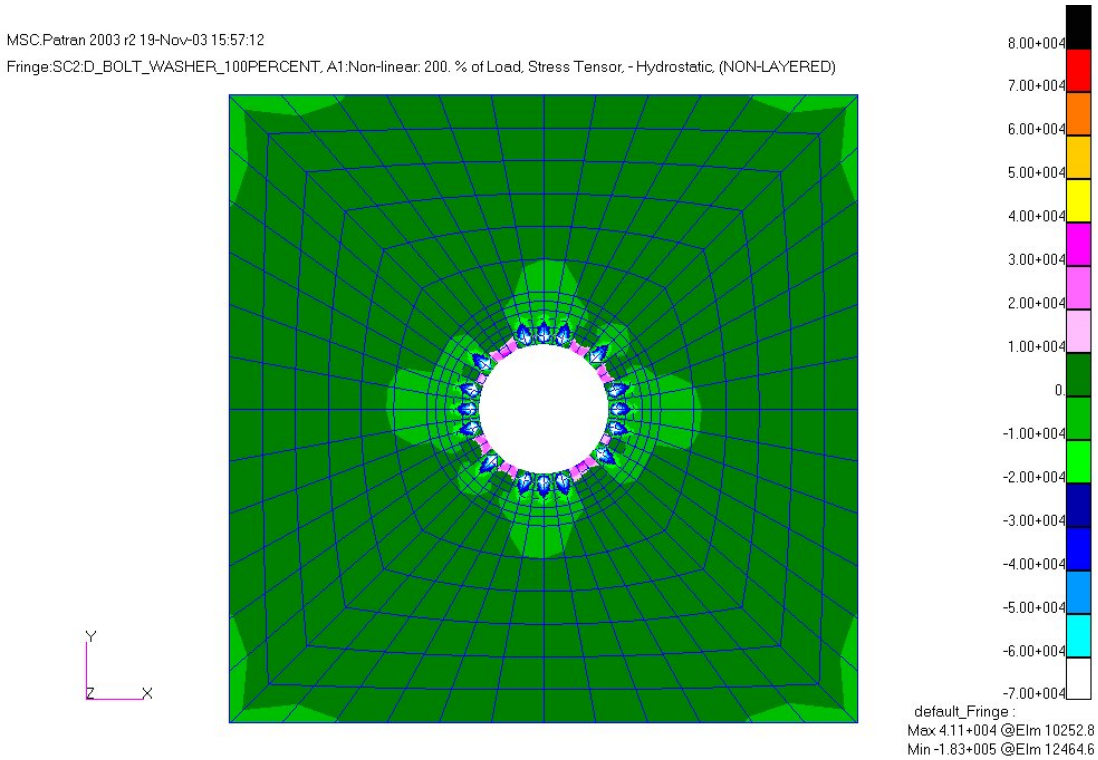

Figure 38: Hi-Lok pre-load with a 0.004 in interference fit, hydrostatic stress contour plot of ½ t plane thickness location.

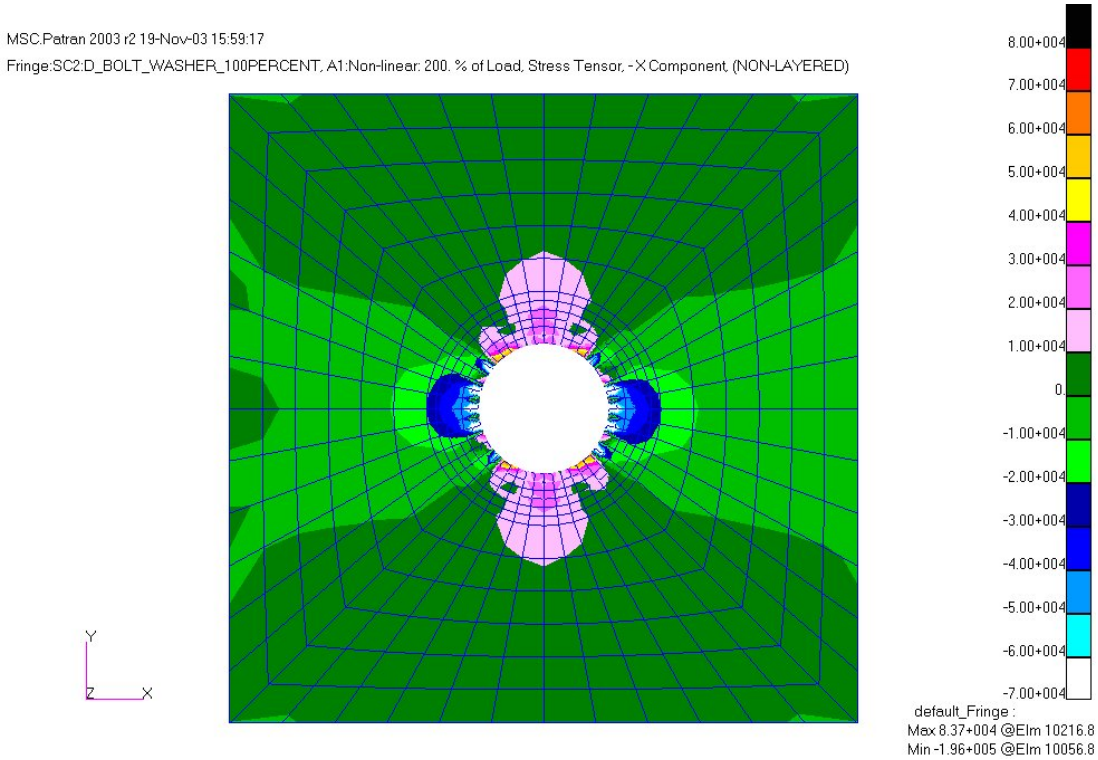

Figure 39: Hi-Lok pre-load with a 0.004 in interference fit, stress tensor x-component contour plot of ½ t plane thickness location.

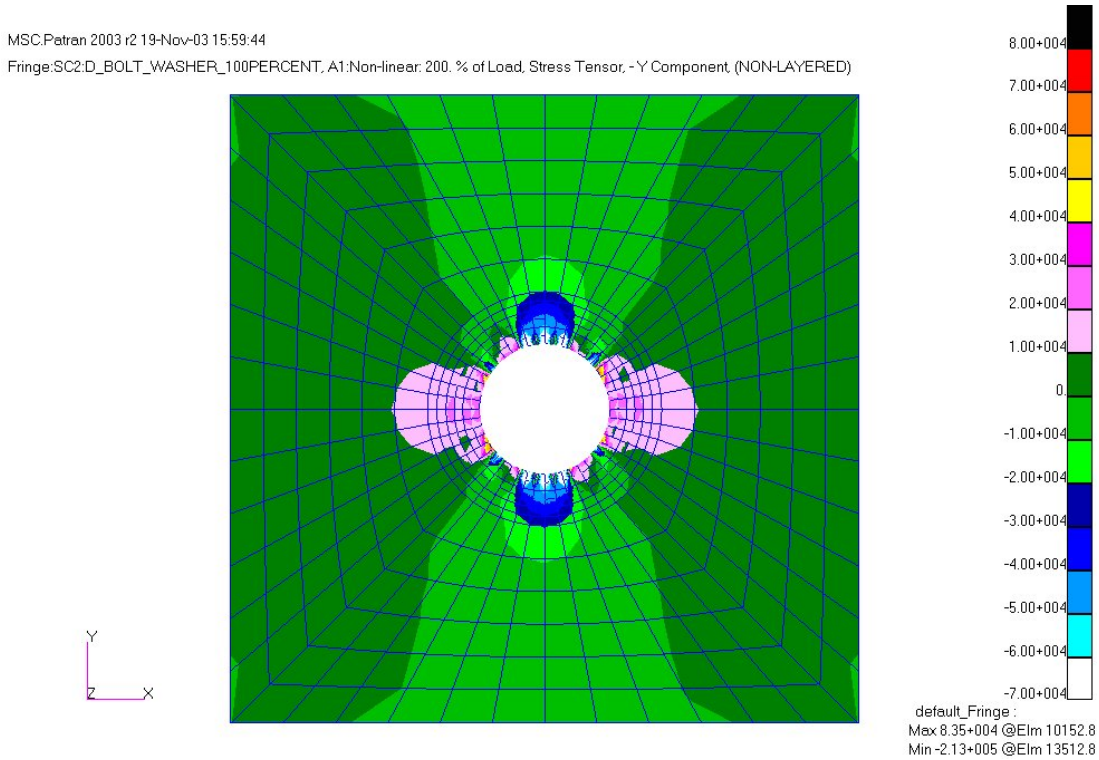

Figure 40: Hi-Lok pre-load with a 0.004 in interference fit, stress tensor y-component contour plot of ½ t plane thickness location.

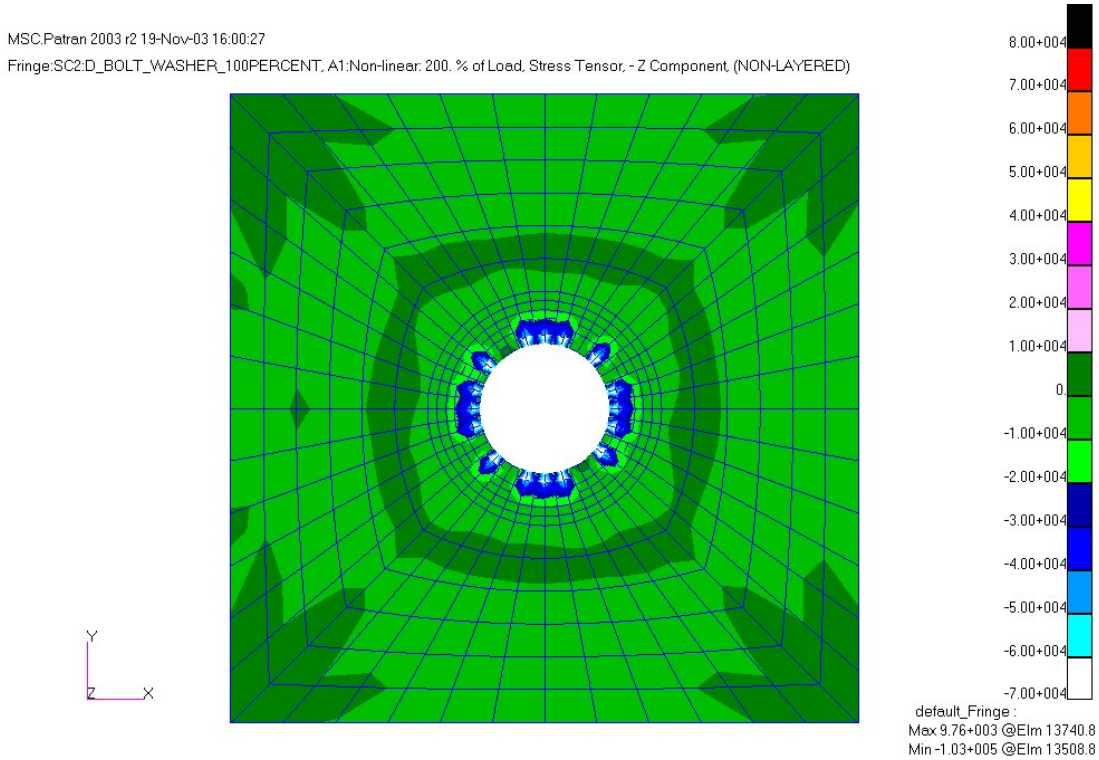

Figure 41: Hi-Lok pre-load with a 0.004 in interference fit, stress tensor z-component contour plot of ½ t plane thickness location.

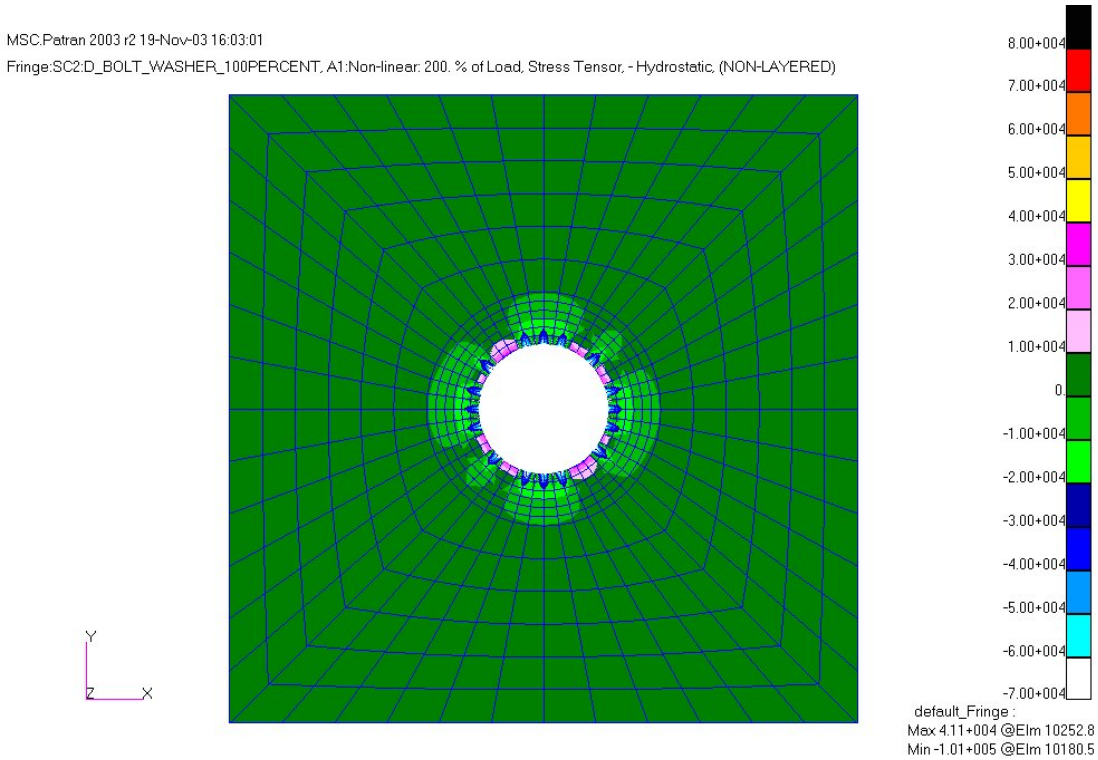

Figure 42: Hi-Lok pre-load with a 0.004 in interference fit, hydrostatic stress contour plot of ¾ t plane thickness location.

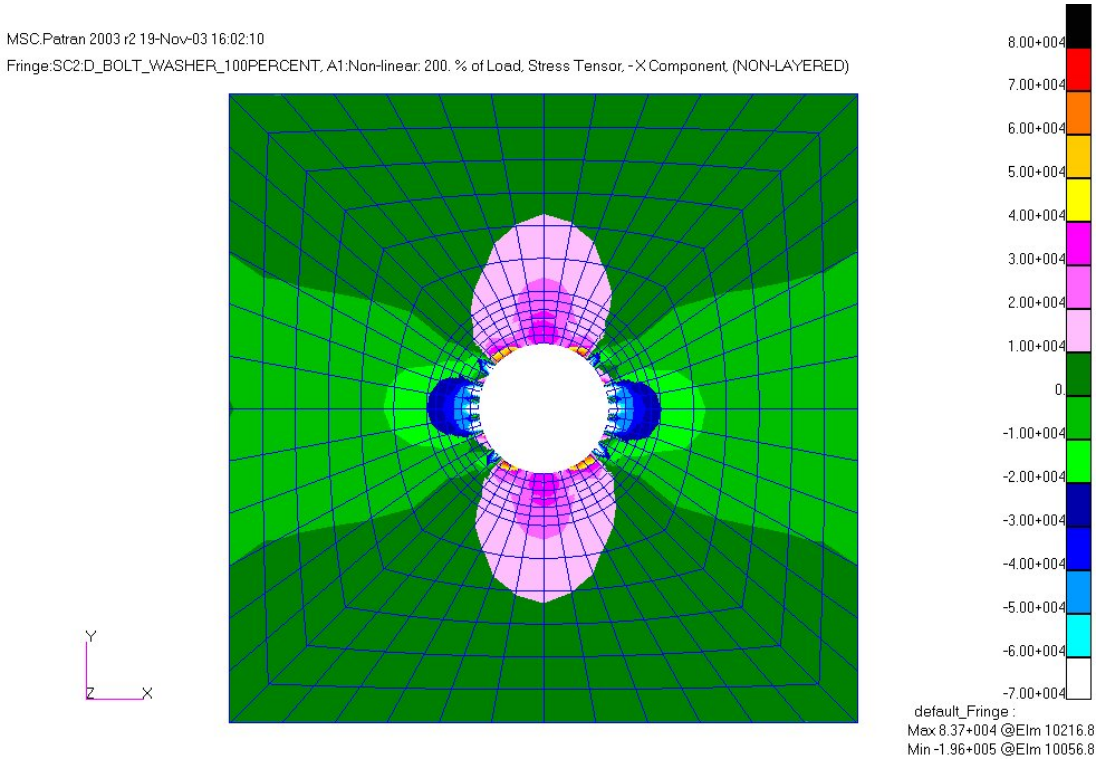

Figure 43: Hi-Lok pre-load with a 0.004 in interference fit, stress tensor x-component contour plot of ¾ t plane thickness location.

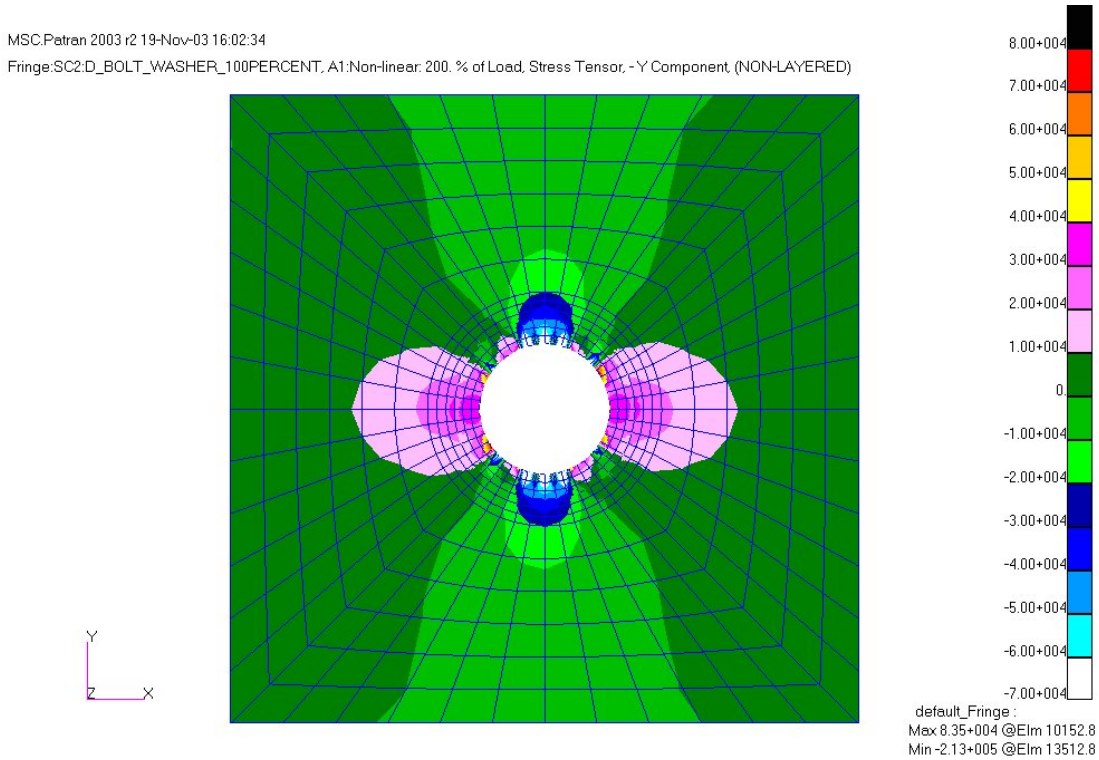

Figure 44: Hi-Lok pre-load with a 0.004 in interference fit, stress tensor y-component contour plot of ¾ t plane thickness location.

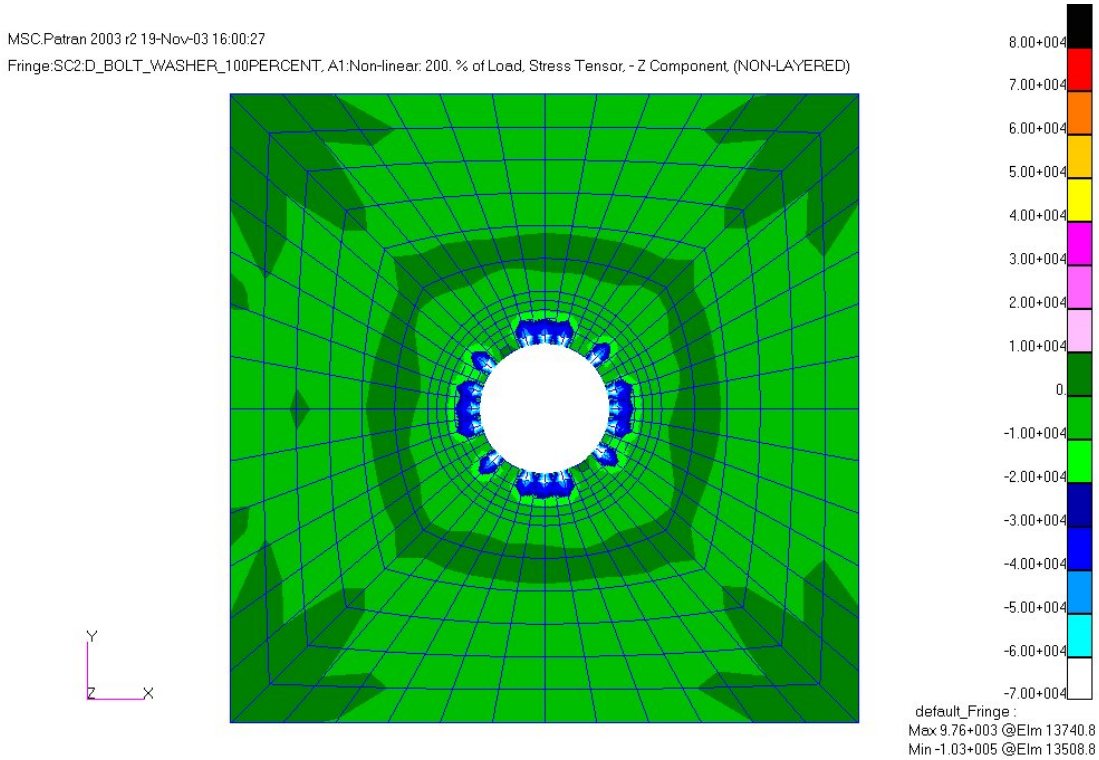

Figure 45: Hi-Lok pre-load with a 0.004 in interference fit, stress tensor z-component contour plot of ¾ t plane thickness location.

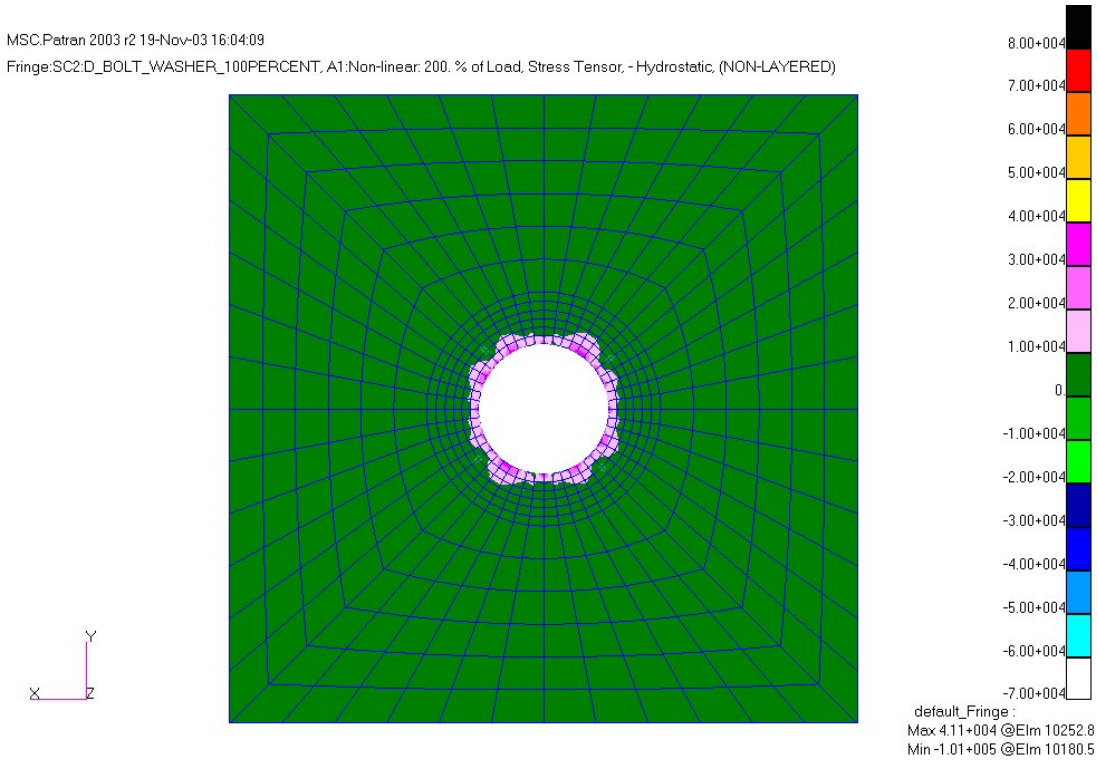

Figure 46: Hi-Lok pre-load with a 0.004 in interference fit, hydrostatic stress contour plot of bottom plane thickness location.

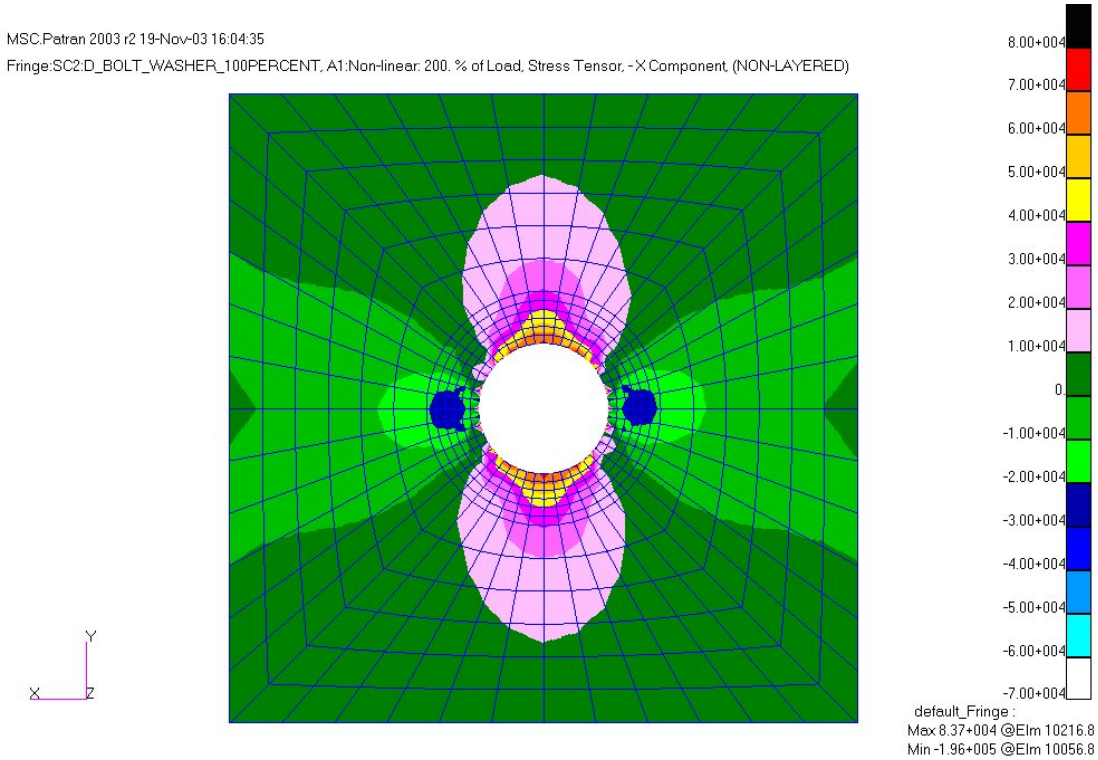

Figure 47: Hi-Lok pre-load with a 0.004 in interference fit, stress tensor x-component contour plot of bottom plane thickness location.

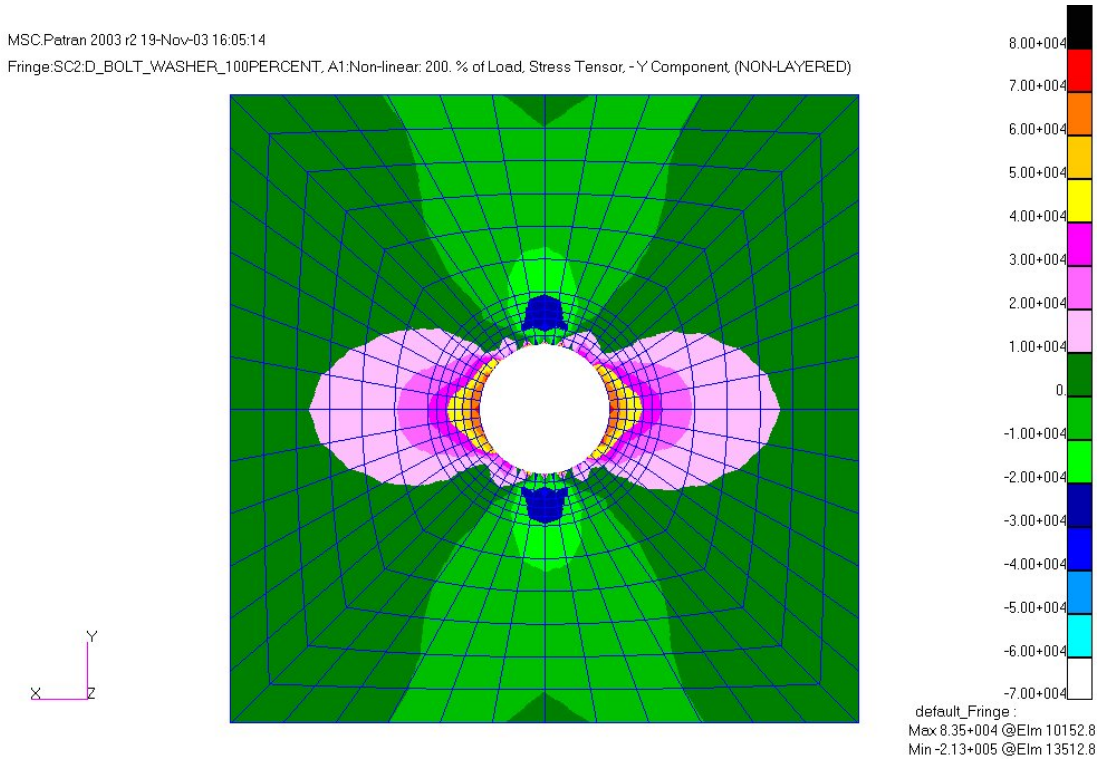

Figure 48: Hi-Lok pre-load with a 0.004 in interference fit, stress tensor y-component contour plot of bottom plane thickness location.

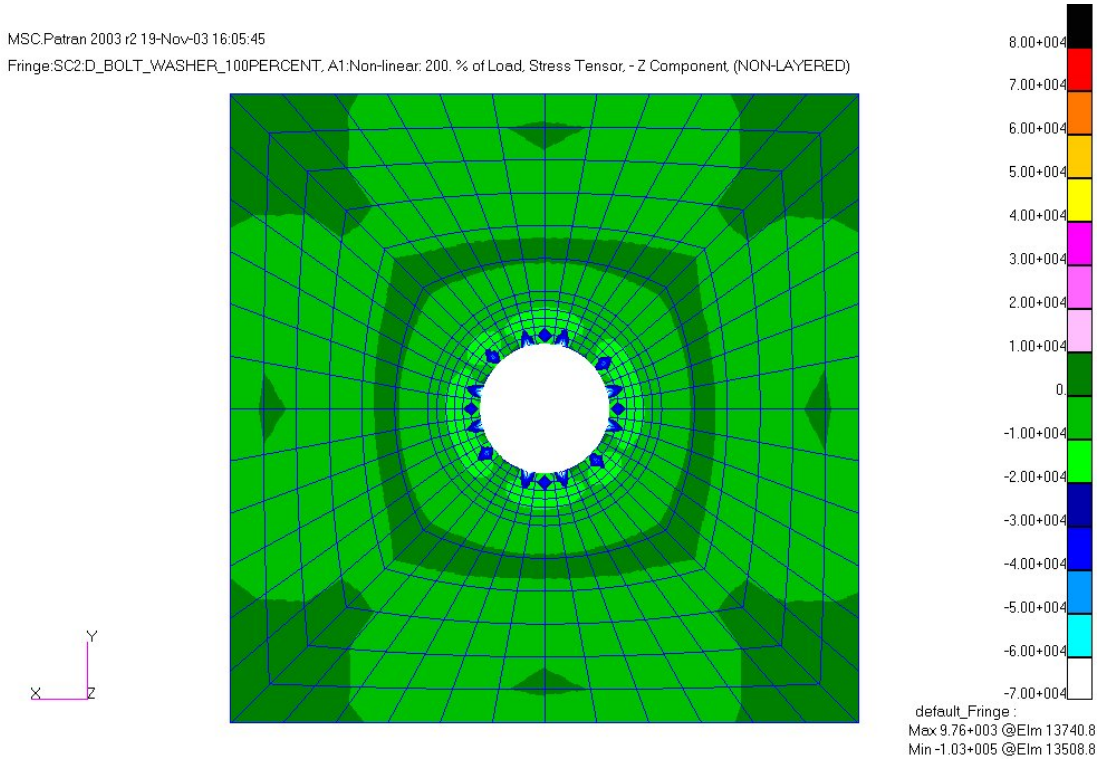

Figure 49: Hi-Lok pre-load with a 0.004 in interference fit, stress tensor z-component contour plot of bottom plane thickness location.

4. Discussion

The results presented in Section 3 represent a small fraction of the available data produced in this work. The volume of the complete stress results for all nodes in the model or even the fastener near field make these data impractical for inclusion in this report. These data are archived in CAStLE and can be made available on CD or similar media. The progress thus far is consistent with expectations for the two types of loads analyzed. The stress tensor, z-component plots show clear evidence of the clamping force provided by the Hi-Lok pre-load. In the interference fit load case the stress imparted to the skin by the pin's interference is also evident. This stress is delivered to the skin surface by means of the sixteen contact slide lines that were defined in the model. Figures 19 to 39 are contour plots of the stress tensor, x-component at the skin mid-plane for clean and interference fit, respectively. Comparing these two Figures the additional stress from the interference fit can be seen concentrated at the lines of contact. While the exact result at the contact lines is suspect due to the clear influence of the stress concentration, there is no reason to doubt the result within a few elements of the surface.

Given the complexity of the model and time consuming nature of contact modeling with MSC/Patran, a traditional degree of freedom versus result convergence study was not practical. Previous work [13] however highlighted the utility of MSC/Patran post processing ***Results*** tools for judging the quality of the solution. The first technique involves disabling one of the tools MSC/Patran uses to make smooth continuous contour plots. MSC/Patran ***Results*** contour plots ordinarily will take the solution for any given node from all its member elements. Then by a choice of averaging schemes creates a single result for that node to give the graphics a single value to plot at each of the 3-D nodal locations. As stated in the previous work, one would expect a convergent solution to have little or no difference between the solutions calculated for any given node from the result for each of the surrounding elements. Stating another way, a poorly converged model with MSC/Patran ***Results*** averaging disabled would indicate large element to element discontinuities in the stress fringe result. In contrast, a well converged solution with averaging disabled would still show a smoothly contoured stress fringe plot.

As an example of this qualitative technique, consider the Hi-Lok pre-load with interference fit load case. Figure 50 shows the result of disabling MSC/PATRAN ***Results*** averaging for this case and plotting the von Mises stress. Von Mises stresses were chosen for this illustration as these are the NASTRAN solution stresses from which all other components are derived. The stress fringe contours shown in Figure 50 are for the most part continuous from element to element. As might be expected, they are most discontinuous between elements that are located at the skin through hole surface. This is especially true near the 16 contact slide line locations—so much so that the slide line locations are easily recognized in the figure. Between the stress concentrations created by the slide lines, the stress not only decreased but a more uniform fringe pattern takes shape. The element to element solution continuity improves considerably within 2 to 3 elements of the hole's surface.

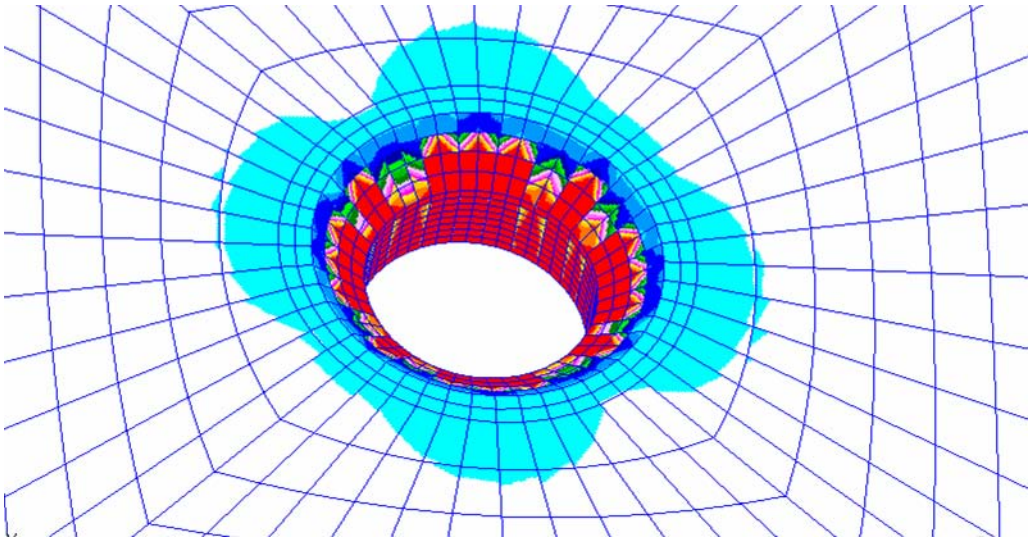

Figure 50: Stress contour plot for Hi-Lok pre-load and interference fit load case with MSC/PATRAN *Results* averaging disabled for the von Mises stress solution.

This same information can be viewed in a different way to obtain somewhat of a quantitative measure of error in the solution. The maximum difference between all element solutions for a given node can also be plotted. Figure 51 is a contour plot result of the stress tensor y-component for the same Hi-Lok pre-load with interference fit load case. The isometric view of the top surface in Figure 51a shows regions of large element to element difference near the lines of contact. With an element to element difference for a given node in the same order of magnitude of the results itself, the precise value of solution in this area should obviously not be trusted. On the other hand, Figure 51b shows the same information at a slice along the x-z plane at y=0 (similar to Section B-B in Figure 1). Evident here is that while the difference near the hole surface is still large, after the first two elements it is generally below 5,000 lb/in^2.

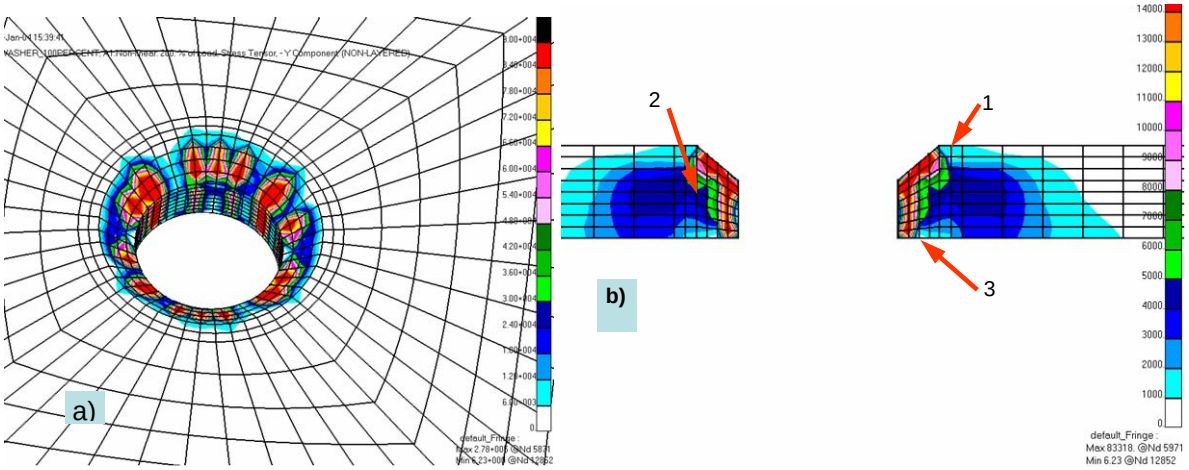

Figure 51: Element to element node solution maximum difference for Hi-Lok pre-load with interference fit load case. Stress tensor, y-component contour plots of a) top view isometric and b) x-z plane at y=0.

Looking in detail at the three points labeled in Figure 51b and comparing with the stress result at that point, the worse case difference is 20% of the result. The percentage is based on

the stress result from the applicable figure which shows the y-component result at that thickness plane. A confidence window as large as 20% would certainly give pause to even the most carefree engineer when applied to a structural sizing effort. But when the interest lies in simply understanding the relative magnitudes and direction of tensile stresses [1] then even this level of accuracy serves the needs of the CESE group when investigating corrosion kinetics in aircraft structure. And this large confidence window is not common to the entire model result as observed in the next two sample points of Figure 51b. Table 4 summarizes the values used for similar confidence calculations for all three points of Figure 51b. It is also worth noting that these values are based on reading the fringe contour plots so the number used is that of the top of the respective fringe color range and therefore a conservative assessment. Finally, large confidence windows such as those of Points 1 and 2 in Table 4 are indicative of the limitations of this sort or contact modeling when using results near those areas of contact.

Table 4: Summary of comparisons between element to element node solutions and the stress result for the same location. Hi-Lok pre-load with interference fit load case.

Point	Maximum difference (Figure 50b), lb/in^2	Stress result, lb/in^2	Figure used to obtain stress result	Maximum difference as a % of stress result
1	2,000	10,000	32	20
2	5,000	30,000	40	16
3	1,000	60,000	48	2

Solution quality (smaller confidence window) while still using MSC/NASTRAN could most likely be improved by adding more lines of contact up to the maximum 48 possible with this mesh. The next level accuracy for this model would likely be obtained by increase the mesh density—particularly near the hole.

5. Conclusion and Recommendations

The work presented here represents a good first order analysis of the complex transition fit fastener contact problem. While the model solution may not have been the highest precision possible, it did meet the immediate needs of the University of Virginia Corrosion Kinetics Team—identification of tensile stress locations and patterns in the fastener near field. The results presented here focused on their specific requirement to identify those stress patterns in the presence of Hi-Lok pre-load and a slight 4 mil (transition) diametric interference fit. The finite element modeling presented here also included the load case appropriate to remote stress on the skin. This last load step was only used to validate the remote stress met the 6-7% load transfer requirement. Further analysis with the load step was withheld for future work. This decision was based largely on the evaluation of model quality with contact slide lines on only one-quarter of the contact surface.

Future work to explore the effect of remote stress will necessitate, at minimum, the inclusion of slide lines on all 48 lines of nodes in the current model. Ideally, the model's element mesh would be redesigned to have a greater element density. This is particularly true within one or two diameters of the hole and particularly in the first two to three elements in the current model. Care must be taken in only increasing mesh density where needed as increased degrees of freedom can negatively impact model convergence.

The above recommendations are the limit of possible improvements using the current MSC/PATRAN 2003 v3 software. While the authors have no experience with the newly released versions, according to MSC engineers the next version of PATRAN will dramatically improve contact modeling. MSC/PATRAN 2004 will permit easy definition of surface to surface contact for preparation of MSC/NASTRAN 2004 analysis decks. Since the change is purely a change of the NASTRAN solver choice, it is expected that the FEM model generations steps outlined here would be very similar. The enhancement was made possible by incorporating a new "solution sequence 600" into the latest version of MSC/NASTRAN. Therefore, this enhance modeling capability also requires the user to also have access to the NASTRAN solution sequence 600 before generating the model with MSC/PATRAN.

In addition to enhanced MSC products there are several other FEM analysis codes that are rumored to be better suited to contact modeling. Future work could include comparison of those codes with the one presented here. HKS/ABAQUS is one such example of an analysis code that is better suited to contact models. The engineer can still take advantage of MSC/PATRAN for easy pre and post processing of the FEM model when using ABAQUS for analysis. The graphical interface make the generation of solid geometry, element mesh, loads and boundary conditions speeds the creation of complex models. MSC/PATRAN post processing also makes interpretation and presentation of the vast arrays of results quick and painless. Whatever the choice, given a more efficient and precise means of defining the contact between model components, tasks such as this would be far less daunting.

6. References

1. Kelly, R. G., e-mail communications to Shoales, 24 November 2003 and 23 December 2003.

2. The Boeing 707 Structural Repair Manual (SRM)

3. HL19 Data Sheet, *Standards Committee for Hi-Lok® Products*, Hi-Shear Corporation, 1992.

4. Scully, J. R., *Air Vehicle Health Management Technical Interchange Meeting*, Dayton, Ohio, 13 November 2003.

5. *PAT301 Introduction to MSC.PATRAN Course Notes*, MSC.Software Corporation, Santa Ana, CA, 2002.

6. Fawaz, S. A., J. Schijve, and A. U. de Koning. "Fatigue Crack Growth in Riveted Lap-Splice Joints." *Proc. of the 19th Symposium of the International Committee on Aeronautical Fatigue*, 16-20 June 1997, Edinburgh, Scot. Scotland, UK: EMAS/SoMat Systems International Ltd, 1997.

7. *MSC.NSATRAN 2004 Quick Reference Guide*, MSC.Software Corporation, Santa Ana, CA, Vol. 2, pp. 982-984, 1606-1609, 2003.

8. Adams, V. and Askenazi, A., *Building Better Products with Finite Element Analysis*, OnWord Press, Santa Fe, NM, pp. 160-166, 1999.

9. Fawaz, S. A., *Thesis Delft University of Technology*, Delft University Press, The Netherlands, pp. 160-161, 164, 1997.

10. Lindeburg, M. R., *Mechanical Engineering Reference Manual for the PE Exam*, 11th Edition, Professional Publications, Inc., Belmont, CA, pp. 51-12:13, 2001.

11. Shigley, J. E. and Mischke, C. R., *Mechanical Engineering Design*, 5th Edition, McGraw-Hill, Inc., New York, NY, pp. 345-347, 1989.

12. *Aluminum Standards and Data 1990*, 10th Edition, the Aluminum Association, Inc., Washington, DC, pp. 119, 121, 1990.

13. Shoales, G. A. and Fawaz, S. A., "Stress Concentration Factor Determination for Various Tensile Test Specimen Configurations by the Finite Element Method using MSC/PATRAN and MSC/NASTRAN," *USAFA 04-03*, USAF Academy, CO, 2004.